NASA CR-174,704

A Reproduced Copy

OF

NASA CR-174, 704

NASA-CR-174704
19840023205

Reproduced for NASA

by the

NASA Scientific and Technical Information Facility

FFNo 672 Aug 65

NASA

THE ANNULAR FLOW ELECTROTHERMAL RAMJET

PREPARED FOR

LEWIS RESEARCH CENTER
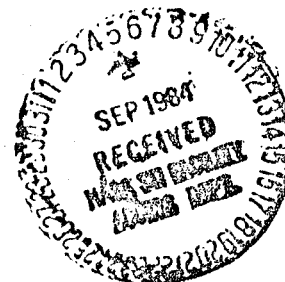
NATIONAL AERONAUTICS AND SPACE ADMINSTRATION

by

Ben D. Shaw

Approved by

Paul J. Wilbur

July 1984

Department of Mechanical Engineering
Colorado State University
Fort Collins, Colorado

N84-31275

1. Report No. NASA CR 174704	2. Government Accession No.	3. Recipient's Catalog No.
4. Title and Subtitle THE ANNULAR FLOW ELECTROTHERMAL RAMJET		5. Report Date July 1984
		6. Performing Organization Code
7. Author(s) Ben D. Shaw Paul J. Wilbur		8. Performing Organization Report No.
		10. Work Unit No.
9. Performing Organization Name and Address Department of Mechanical Engineering Colorado State University Fort Collins, Colorado 80523		
		11. Contract or Grant No NGR-06-002-112
12. Sponsoring Agency Name and Address National Aeronautics and Space Adminstration Washington, D.C. 20546		13. Type of Report and Period Covered
		14. Sponsoring Agency Code

16. Abstract

The annular flow, electrothermal, plug ramjet is examined as a possible means of achieving rapid projectile acceleration to velocities for such applications as direct launch of spacebound payloads. The performance of this ramjet operating with hydrogen propellant is examined for cases where this working fluid is treated (1) as a perfect gas and (2) as a gas that is allowed to dissociate and ionize and then recombine with finite reaction rates in the nozzle. Performance results for these cases are compared to the performance of a conventional ramjet operating with perfect gas hydrogen propellant. It is shown that the performance of the conventional ramjet is superior to that of the annular flow, electrothermal ramjet. However, it is argued that the mechanical complexities associated with conventional ramjet operation are difficult to attain, and for this reason the annular flow, electrothermal ramjet is more desirable as a launch system. Models are presented which describe both electrothermal plug ramjet and conventional ramjet operation, and it is shown that for a given flight velocity there is a rate of heat addition per unit propellant mass for which ramjet operation is optimized. In general, dissociation and ionization losses in the hydrogen propellant are found to be small and nozzle flow is shown to be near chemical equilibrium rather than a chemically frozen state. It is demonstrated that diffuser shock losses, while significant, do not degrade performance to unacceptably low levels. Data are presented in such a way that they can be used in analyzing various mission profiles. It is demonstrated that the residence times of fluid particles within the electrothermal plug ramjet are small compared with the times required for flowfield changes to be significant. It is argued therefore that errors introduced by assuming quasi-steady flow are not excessive. The thermal efficiencies over different launch cycles are shown to be high (between 30% and 40%), and the pressure, temperature and power demand requirements are demonstrated to be reasonable.

17. Key Words (Suggested by Author(s)) Ramjet Direct Space Launch Hydrogen	18. Distribution Statement Unclassified - Unlimited		
19. Security Classif. (of this report) Unclassified	20. Security Classif. (of this page) Unclassified	21. No. of Pages 104	22. Price*

* For sale by the National Technical Information Service, Springfield, Virginia 22161

TABLE OF CONTENTS

LIST OF FIGURES

NOMENCLATURE

A = flow area, m^2

d = diameter, m

F = thrust, N

g = acceleration due to gravity, 9.8 m/s^2

M = Mach number

P = static pressure, Pa

P_T = stagnation pressure, Pa

$\dot{Q}$ = heat addition rate, w

q = heat addition per unit mass, J/Kg

T = static temperature, $^\circ K$

T_T = stagnation temperature, $^\circ K$

V = velocity, m/s

δ = conical diffuser half-angle, degrees

γ = ratio of specific heats

ρ = density, Kg/m^3

σ = acceleration, g's

K_1, A, B, C, D = constants used in Eqs. 8, 9, 10, and 11

A numerical subscript on a variable corresponds to a fluid state
defined in Figure 3a and/or 3b.

INTRODUCTION

Direct launch systems are currently being considered for space re-
supply and disposal missions where high accelerations can be tolerated.
Payloads delivered into space with these systems would be accelerated
to very high velocities (on the order of 10^4 m/sec) close to the earth's
surface and they would then be slowed somewhat to the desired final
energy during passage through the earth's atmosphere. One such system
that has been proposed recently for such missions is the electrothermal
ramjet.[1] This system appears to be capable of achieving the high ac-
celeration levels needed to assure launch tracks that are of a reason-
able length primarily because it does not accelerate either the
propellant or the power plant required to effect its operation.

Conceptually the electrothermal ramjet involves a long tube filled
with gaseous propellant through which a ramjet engine is accelerated to
a specified terminal velocity. Typically the ramjet would be operated
at constant thrust using hydrogen propellant heated by either electro-
magnetic radiation or electrical currents as it passes through the
ramjet. Energy would either be beamed or conducted to the ramjet heat
addition zone from the tube walls as the ramjet passed down the launch
tube. Because a ramjet requires a substantial initial velocity before
it can begin to produce thrust it is anticipated that the ramjet would
be accelerated to this velocity by a device such as a light gas gun.
Preliminary analysis[1,2] has suggested that a particular ramjet design
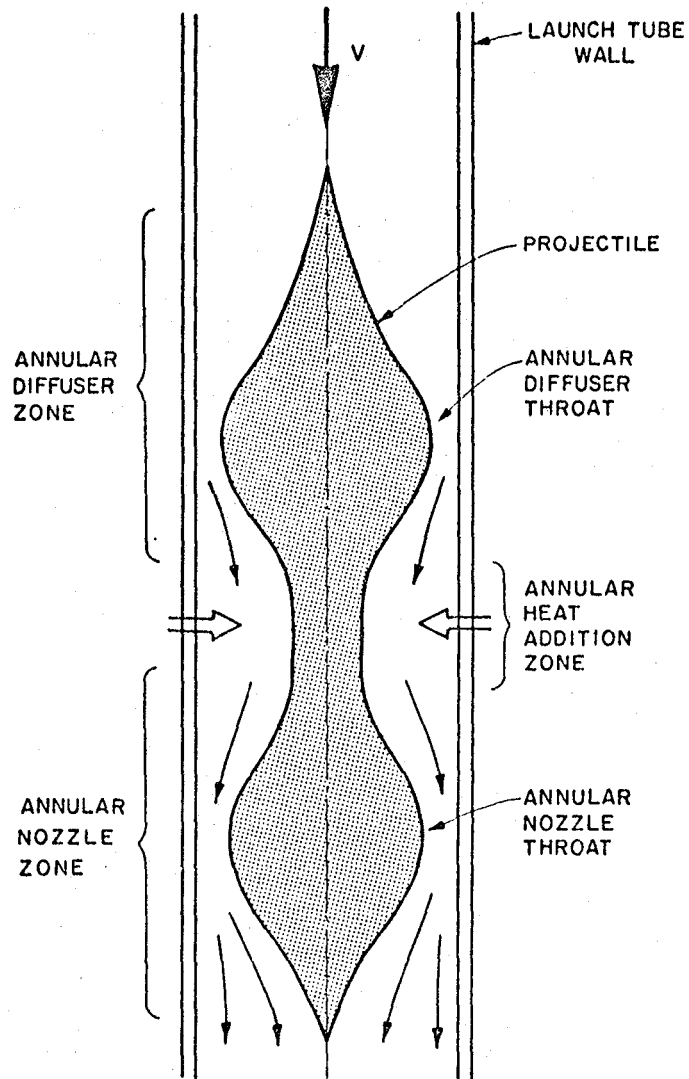
Fig. 1   Electrothermal Ramjet Concept

referred to as the annular flow, plug ramjet is well suited to this application and that such a device should exhibit good performance.

The general concept of the electrothermal plug ramjet is shown in Fig. 1. The projectile, which is a solid centerbody, is shown traveling down the circular tube. The reference frame is chosen to be moving with the projectile so the gaseous propellant is shown moving towards the projectile with velocity V. The incoming propellant will encounter the annular diffuser where it will be slowed relative to the projectile. The coupling of the tube wall with the projectile forebody will produce the geometric configuration necessary to bring the propellant to subsonic conditions at the exit of the annular diffuser zone. After the propellant has been brought to subsonic conditions, heat is added in the annular heat addition zone, and the propellant then passes through the annular nozzle zone, which is a converging-diverging channel, and is expelled out the rear of the device so as to produce a thrust force on the projectile. This annular design is utilized because it has several attractive features including

1) Heat addition can be effected outside the ramjet body directly from the tube wall. This eliminates the need for windows in the ramjet body for the case of beamed energy heating and sliding current contacts for arc discharge heating schemes.

2) Direct mechanical or fluid mechanical forces induced between the tube wall and the projectile should tend to stabilize and center it.

3) The structural design of the projectile appears to be relatively simple.

4) Shock losses in the diffuser can be minimized by properly

designing the annular diffuser section.

5) There will be no "spill over" of propellant.

6) Variations in fluid flow areas needed to achieve proper flow conditions as the projectile velocity increases can be achieved by varying the cross-sectional area of the launch tube as a function of axial position.

Preliminary analyses regarding annular flow electrothermal ramjet operation have been conducted[1,2] and typical results obtained from these studies showing design and operating parameters for a typical mission are presented in Figure 2. These results assume that there are no diffuser shock losses, that the hydrogen propellant behaves as a perfect gas, and that the fluid flow is quasi-steady. These results detail the performance of a ramjet launch cycle for the following specific operational parameters

1) A constant projectile mass of 10 kg.

2) A constant acceleration of 30,000 g's (hence constant thrust) from rest to 15,000 m/s.

3) An initial propellant temperature of 300°K.

4) An initial propellant pressure of 30 atm.

5) A fixed projectile diffuser throat diameter of 16 cm (Fig. 1).

6) A fixed projectile heat addition zone diameter of 8 cm (Fig. 1).

If one assumes that the projectile will be acted upon by either the ramjet force or some externally applied force needed to produce the desired acceleration, the projectile trajectory will be known. With the projectile velocity profile known, the propellant flow velocity relative to the ramjet is known at each position along the launch track. One can now prescribe the diffuser throat area required at each position along

$\sigma_f = 30000$ G's
$m_f = 10$ kg
$T_1 = 300°K$
$P_1 = 30$ atm
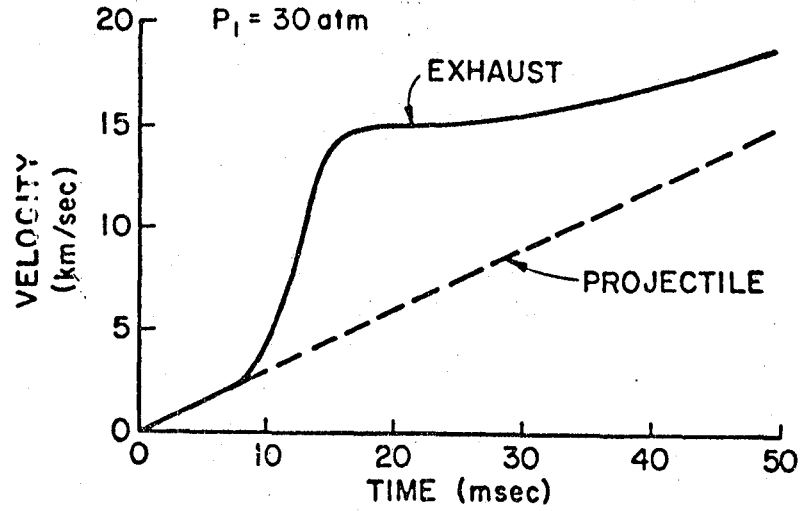
a. Velocity Profiles
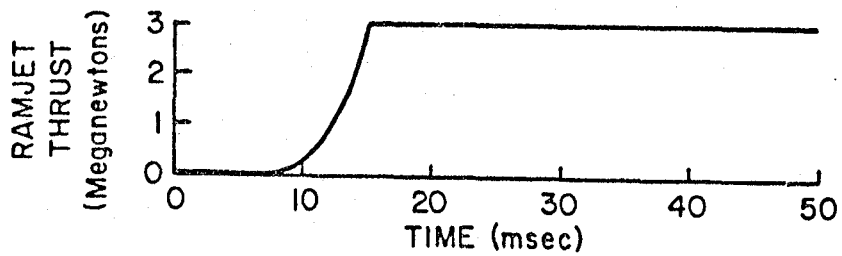
b. Thrust Profile

Fig. 2 Typical Electrothermal Ramjet Launch Profile
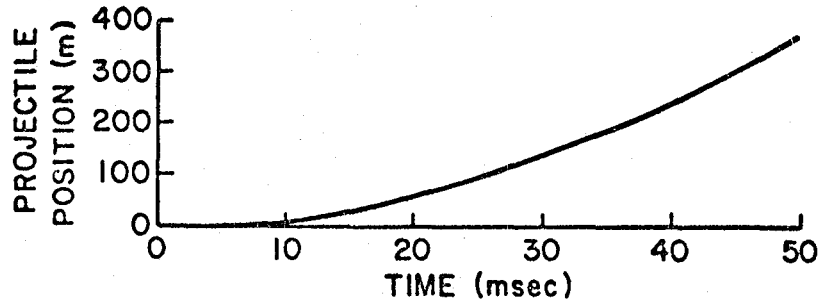
c. Projectile Position Profile
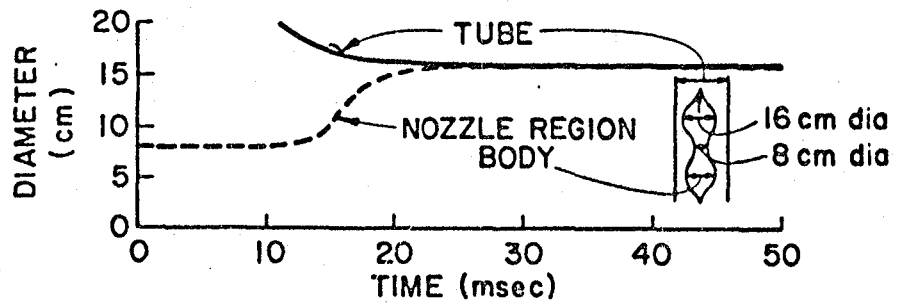
d. Projectile and Tube Diameter Profiles

Fig. 2 Typical Electrothermal Ramjet Launch Profile
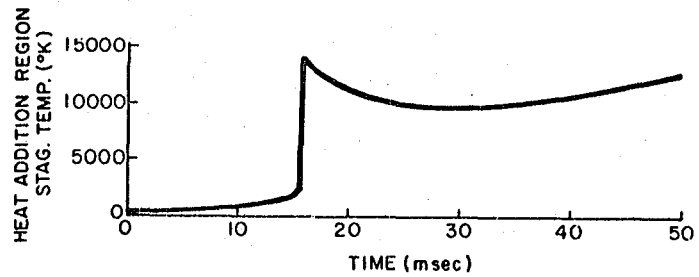
e. Heat Addition Stagnation Stagnation
   Temperature Profile
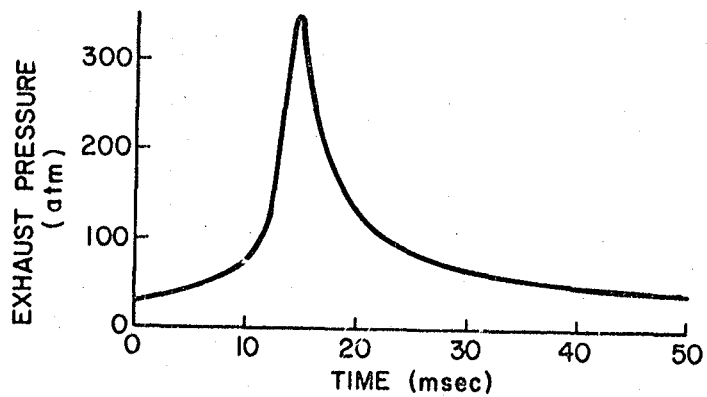
f. Exhaust Static Pressure Profile

Fig. 2 Typical Electrothermal Ramjet Launch Profile
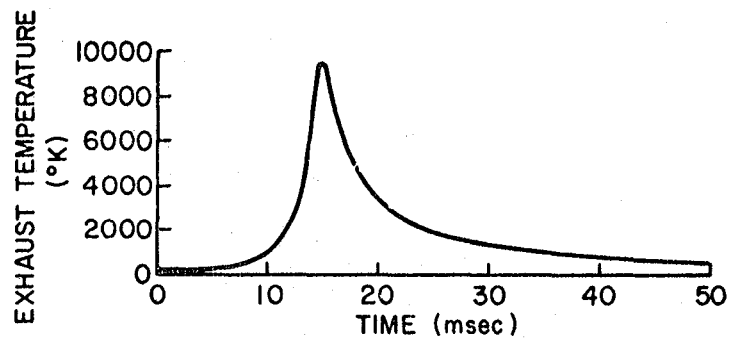
g. Exhaust Static Temperature Profile
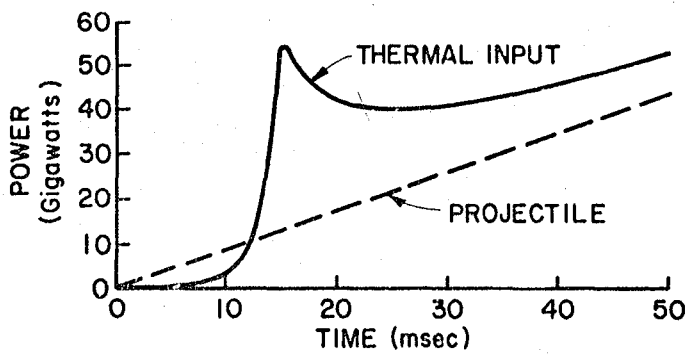
h. Thermal Input and Power Into Projectile
Acceleration Profiles

Fig. 2 Typical Electrothermal Ramjet Launch Profile

the tube so that the flow will remain sonic at this throat. One can also prescribe the heat supplied in the subsonic heat addition region so that the specified thrust will either be produced or the Mach number at the exit of the heating region (in the projectile frame of reference) reaches its maximum allowable value of unity. After heat has been added, the flow is accelerated isentropically in the nozzle to the maximum supersonic Mach number achievable under the constraint of the area change available. The static pressure at the nozzle exit is determined by this expansion and it will vary with projectile position. Proper control of this pressure at the base of the projectile would have to be achieved in an actual device by proper design of the launch tube. Such a tube would consist of two sections: a cavity section into which hydrogen processed by the ramjet would be collected, and the launch section through which the projectile would pass. It has been assumed in this analysis that the cavity section could be designed to have the length and cross-sectional area needed to accommodate the propellant and facilitate maintenance of the necessary projectile base pressure. While it seems possible to do this intuitively, the examination of the unsteady fluid mechanics describing the process has not yet been attempted.

Figure 2 shows the results of such an analysis for the case where a constant thrust of 3×10^6 N is maintained on a 10 kg mass. As Fig. 2a shows, the projectile velocity (in the launch tube frame of reference) increases linearly with time. Since the propellant is initially at rest relative to the tube wall the projectile velocity is equal to the propellant inlet velocity in the projectile frame of reference. The exhaust velocity (in the projectile frame of reference) is observed to be equal to the inlet velocity during the first ~ 8 ms of operation, so

during this time interval, essentially no net thrust is produced through the mechanism of momentum change of the propellant. After about 16 ms of operation, however, the exhaust velocity has risen to about 15 km/s and has begun to level off. During the time between $\sim$ 8 and $\sim$ 16 ms, all of the heat that can be added without choking the flow (achieving unity Mach number at the end of the heat addition region) is being added.

As Fig. 2b shows, the net ramjet thrust is inadequate to meet the 3×10^6 N thrust requirement at times less than 16 ms. Thus an alternative accelerating scheme, such as the light gas gun[3] would have to be used during this time interval. As the projectile velocity increases, more heat can be added and this causes the increase in exhaust velocity shown in Fig. 2a. After $\sim$ 16 ms, both the exhaust velocity and the mass flow rate have risen to the point where the desired thrust level can be produced and the Mach number after heat addition begins to drop below unity.

Figure 2c, which indicates projectile position as a function of time for this case of constant acceleration, shows a launch tube about 400 m long would be required to accelerate the 10 kg mass to the terminal velocity of 15,000 ms in $\sim$ 50 ms. Figure 2d shows the variation in tube and projectile diameters that would have to be effected to satisfy fluid mechanical constraints imposed on the ramjet. As previously stipulated, the projectile diameters at the diffuser throat and in the heat addition region have been treated as fixed at 16 and 8 cm respectively. The reduction in tube diameter required to yield unity Mach number at the diffuser throat as the projectile velocity increases is shown by the solid line. Data from this line taken together with the position

profile of Fig. 2c specify how the tube diameter would have to vary along its length. Figure 2d also shows that the projectile diameter at the nozzle throat would have to increase as the projectile velocity increases and the input power is varied to induce the desired thrust level. The fact that this diameter must change during the launch cycle represents a significant mechanical complication in the system. It is noted, however, that the amount of change in this diameter becomes very small after about 20 ms when the projectile velocity is $\sim$ 5 km/s. It is anticipated that a pressure- or temperature-sensitive scheme might be designed to facilitate this change in projectile diameter at the nozzle throat. Alternatively, one could hold the projectile diameter in the nozzle region fixed, reduce the tube diameter slightly more rapidly than Fig. 2d suggests, and abrade the diameter of the projectile at the diffuser throat using protrusions from the tube wall.

Figures 2e, 2f, and 2g indicate how the stagnation temperature in the heat addition zone and the static pressure and temperature at the nozzle exit should vary to conform to the problem specifications. The peaks in temperature and pressure occur at the point where the power input is a maximum (Fig. 2h). This, in turn, occurs at the time when the thrust has just reached its design value and the Mach number at the end of the heat addition region is still at unity. At this condition, the exhaust velocity is still relatively low and the bulk of the thrust is being produced by the static pressure difference across the projectile. If one did not start using the ramjet until after $\sim$ 20 ms into the launch, the exhaust pressure and temperature would lie in a very moderate range throughout the period of ramjet operation. Note that it is the pressure profile of Fig. 2f that would have to be matched

through proper design of the cavity section of the launch tube. This might be achieved by selecting not only the length and cross-sectional area of this section, but also by the inclusion of accumulator chambers that could be connected into the tube at the proper time.

The heat addition zone stagnation temperature (Fig. 2e) is observed to remain near 10,000°K after about 16 ms. It is noted that dissociation and ionization may introduce significant effects while operating within this regime, and these effects will be examined later in this analysis.

Figure 2h shows the thermal power input profile required to effect operation as well as the actual profile of mechanical power input to the projectile. After the $\sim$ 20 ms period over which the auxiliary starting force would be applied, it is observed that the ratio of projectile power to thermal input power rises above $\sim$ 50%. The ramjet is observed to become increasingly efficient as the launch cycle proceeds. This suggests that the ramjet will be more efficient at the higher velocities, where the efficiencies of electromagnetic launchers drop off. The difference between the projectile and thermal input powers represents the power being deposited as kinetic and thermal energy in this hydrogen propellant. It should be noted here that frozen flow losses in the nozzle and electrical-to-thermal power conversion losses as well as frictional losses have been neglected in this preliminary analysis.

The results presented in Fig. 2 suggest that the annular flow electrothermal ramjet concept has the potential of achieving efficient high velocity high acceleration launches, and also that this concept cannot be rejected on the basis that it violates a basic principle of fluid mechanics or thermodynamics. The pressure, temperature and power

demand profiles are all reasonable, and it is for these reasons that
further analysis of the annular flow electrothermal ramjet was under-
taken to bring to light aspects which may degrade ramjet performance.

There are several effects which may degrade plug ramjet performance
below that shown in Figure 2. Some of these effects are

1) Diffuser shock losses.

2) Propellant dissociation, ionization and non-perfect modes of
molecular and atomic energy storage.

3) Freezing (translational, rotational, vibrational, chemical).

4) Non-steady gas dynamics effects.

It is the purpose of this thesis to address these effects and to de-
termine the magnitude of degradation of annular flow electrothermal
ramjet performance that they might cause.

In order to illustrate the performance of the electrothermal plug
ramjet, an analysis will be also conducted on the more familiar con-
ventional ramjet which uses hydrogen propellant that behaves as a
perfect gas. The results from this analysis will be compared to analyses
conducted for the annular flow electrothermal plug ramjet. Simple
theoretical models detailing conventional ramjet and electrothermal
ramjet operation with perfect gas hydrogen propellant will be presented,
and data from the more extensive analyses considering dissociation,
ionization and non-equilibrium processes will be interpreted in the
light of the results from the simplified models.

It should be stated here it has been assumed in all analyses that
the fluid flow is axis-symmetric or one-dimensional and quasi-steady,
and the fact that the tube wall is moving in the reference frame of
the annular flow electrothermal plug ramjet is assumed to have no

influence on the flow. All flowfields analyzed are considered to
be inviscid. The ideal gas equation of state is assumed to be valid
at all times.

FLOWFIELD MODELS

The general concept of a conventional ramjet is shown in Fig. 3a.
The reference frame is chosen to be moving with the ramjet, so the pro-
pellant is shown moving towards the inlet with a velocity V_1. The Mach
number associated with the incoming flow is designated M_1. After the
ramjet has been accelerated to a high enough initial velocity, an ob-
lique shock will be attached to the conical tip of the center body
which serves as a diffuser. Downstream of the diffuser tip, a series
of shocks reflected between the center and outer bodies will occur.
They will terminate in a normal shock that will slow the flow to sub-
sonic conditions. A review of the hypersonic wind tunnel literature[4]
has suggested that normal shock recovery can be expected after the
initial conical shock, so it is assumed that the flow passes through an
initial conical shock to State 2 and then passes through a single nor-
mal shock to State 3. One-dimensional values obtained by averaging
over the axis-symmetric conical flow field variables computed at the
exit to the conical flow field in Region 2 are used as input for the
normal shock relations. For a description of the methods used to com-
pute the average conical flowfield values see Appendix A.

Across the normal shock, equations describing mass continuity, the
first law of thermodynamics, conservation of momentum, and the second
law of thermodynamics are satisfied. Immediately downstream of the
normal shock it is assured that the area between the center and outer
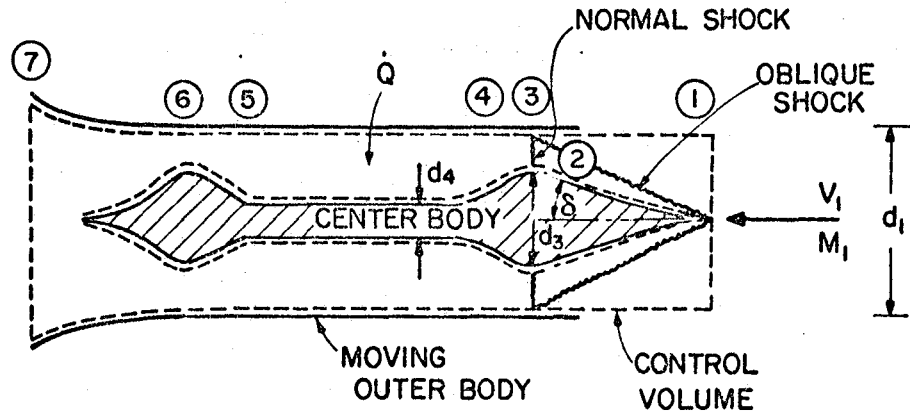
a. CONVENTIONAL RAMJET
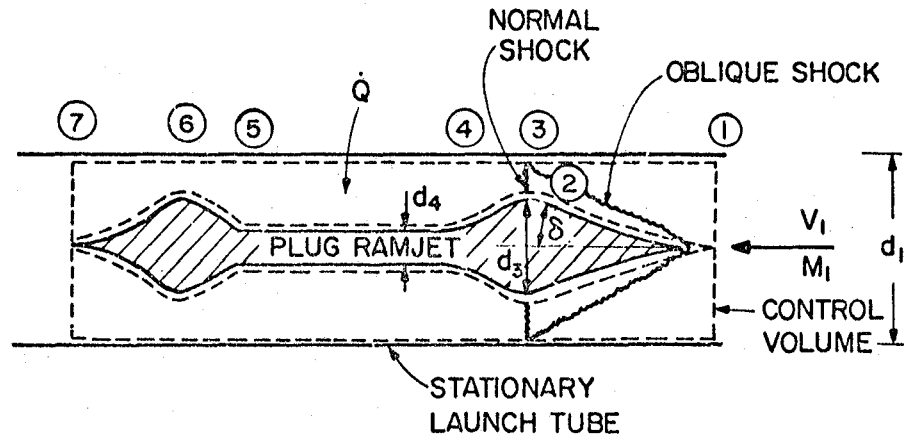
b. ELECTROTHERMAL ANNULAR FLOW RAMJET

Fig. 3 Ramjet Configurations

bodies is sufficient so the flow will pass through the minimum area
that is encountered at the diffuser throat. After the normal shock,
the flow enters the subsonic heat addition region at 4 and heat is
assumed to be deposited into the flow between States 4 and 5. In the
heat addition region, the first and second laws of thermodynamics are
satisfied, along with mass continuity and the momentum equation. After
leaving the heat addition region at 5, the flow passes through a
converging-diverging channel where it is accelerated first to the sonic
condition at state 6 and then on to supersonic conditions at the nozzle
exit 7. No

With this conventional ramjet (Figure 3a) the static inlet and
outlet pressures are equal because the free stream conditions are com-
municated outside of the moving outer body. In order to satisfy this
condition while assuming no shocks in the nozzle one finds the nozzle
exit area (A_7) must be larger than the free-flow diffuser inlet area
(A_1). It is hoped that by comparing this more familiar ramjet to the
new one being proposed that the concept and performance of the plug
ramjet can be better understood.

The annular flow plug ramjet is shown in Fig. 3b. It appears
similar to the conventional ramjet at first glance, but is different in
the following ways

1) The plug ramjet moves down the tube as the center body of the
conventional ramjet does but in the plug ramjet case the outer
body is the launch tube which is stationary. Because the
launch tube diameter is essentially constant along its length
the fluid mechanics and thermodynamics of the problem can be
considered from the frame of reference of the ramjet as though

this tube were not moving.

2) The inlet and outlet areas associated with flow through the plug ramjet (A_1 and A_7) must be equal, again because the launch tube diameter does not vary significantly along its length.

3) The inlet and outlet pressures P_1 and P_7 are not equal because the upstream and downstream regions are not connected through an exterior path. In fact the outlet pressure P_7 will be greater than the inlet pressure P_1 and this pressure difference will therefore produce some component of the thrust exerted on the plug.

One can see that the fluid mechanics of both configurations in Figs. 3a and 3b are described by the same basic equations. The only difference in the two cases is the difference in the boundary conditions that are applied to the flow.

When non-perfect gas modes of energy storage such as ionization and dissociation are allowed to occur, results from statistical mechanics are utilized to compute equilibrium compositions and thermodynamic properties and shifting chemical composition is allowed to occur. For a description of the methods used to compute the equilibrium properties of hydrogen see Appendix B. Where they are deemed potentially important, nonequilibrium processes are evaluated by considering finite rate reactions and by calculating the conditions at which specific reactions will become slow enough so the chemical composition of the flow becomes essentially frozen. A description of the methods utilized to perform these calculations can be found in Appendix C.

Because the essense of the phenomena occurring in ramjet devices of the types considered here can be described by simple, perfect gas

models, these types of theoretical models will be presented to illustrate the basic operational trends present in the analyses conducted.

Perfect Gas Models

Consider now that either ramjet in Fig. 3 is being accelerated at a constant thrust F and that heat is being added at a rate $\dot{Q}$ to achieve this level of thrust. In general $\dot{Q}$ will vary with the velocity of the ramjet and will be different for the conventional and plug designs. By assuming that the propellant flowing through the control volumes shown in Figs. 3a and 3b behaves as a perfect gas, the momentum equation applied across the control volumes of Fig. 3 can be put in the following form

$$\frac{F}{P_1 A_1} = \frac{A_7}{A_1} \frac{P_{T_7}}{P_{T_1}} \left[\frac{1 + \frac{\gamma-1}{2} M_1^2}{1 + \frac{\gamma-1}{2} M_7^2} \right]^{\frac{\gamma}{\gamma-1}} [\gamma M_7^2 + 1] - [\gamma M_1^2 + 1] . \tag{1}$$

In this equation the entrance and exit conditions are respectively; Mach number M_1, M_7; area A_1, A_7 and stagnation pressure P_{T_1}, P_{T_7}. The ratio of specific heats is γ and P_1 represents the entrance static pressure. The left hand side of this equation represents a non-dimensionalized thrust. The stagnation pressure ratio appearing in Eq. 1 can be written

$$\frac{P_{T_7}}{P_{T_1}} = \frac{P_{T_4}}{P_{T_1}} \frac{P_{T_5}}{P_{T_4}} \frac{P_{T_7}}{P_{T_5}} \tag{2}$$

where (P_{T_4}/P_{T_1}), the stagnation pressure ratio across the diffuser, is less than unity because of diffuser losses. The heat addition region stagnation pressure ratio (P_{T_5}/P_{T_4}) is also less than unity because of heat addition-induced stagnation pressure losses. Because the nozzle is assumed to be isentropic the ratio (P_{T_7}/P_{T_5}) is unity.

When the first law of thermodynamics is applied to a perfect gas working fluid, the following expression for the instantaneous ramjet efficiency (power into ramjet mass acceleration divided by input thermal power) is obtained

$$\frac{FV_1}{\dot{Q}} = \frac{F}{P_1 A_1} \frac{\gamma-1}{\gamma} \left[(1 + \frac{\gamma-1}{2} M_1^2)(\frac{T_{T_7}}{T_{T_1}} - 1) \right]^{-1} . \qquad (3)$$

To apply these equations to the analysis of either ramjet it is necessary to specify the inlet Mach number (M_1) and the diffuser geometry so that the diffuser stagnation pressure ratio (P_{T_4}/P_{T_1}) can be computed. For a given conical diffuser half-angle (δ) and annular diffuser shoulder diameter (d_3) and heat addition center body diameter (d_4) the inlet free-flow diameter (d_1) is specified by placing the intersection of the conical shock and the outer body or tube wall at the annular diffuser shoulder. Specifying these parameters serves to fix the flow conditions up to State 4, where subsonic conditions are always specified.

The flow downstream of the conical flowfield is assumed to be one-dimensional, so one-dimensional values for the conical flowfield variables are computed by the methods detailed in Appendix A. These one-dimensional values of the variables are then used as input to the normal shock relations so the stagnation pressure ratio P_{T_4}/P_{T_1} and the flow conditions downstream of the normal shock at 3 can be utilized to specify the conditions at the entrance to the heat addition region 4. By knowing M_4 and specifying M_5, the heat addition stagnation pressure ratio (P_{T_5}/P_{T_4}) is fixed, as is the stagnation temperature ratio ($T_{T_5}/T_{T_4} = T_{T_7}/T_{T_1}$). To analyze ramjet operation then, either the

exit/inlet area ratio (A_7/A_1) or the exit/inlet static pressure ratio (P_7/P_1) may be specified to fix M_7. For the conventional ramjet the pressure ratio P_7/P_1 is set to unity, and for the electrothermal ramjet the area ratio A_7/A_1 is set to unity. It is noteworthy that the parameters A_7/A_1, P_7/P_1 and M_7 are not completely independent. Specifying one parameter dictates values for the others.

Dictating the exit/inlet conditions for the ramjet control volume allows the calculation of other parameters such as the exit/inlet velocity and temperature ratios, and the fractions of the total thrust provided by 1) the difference in the pressure area product between the entrance and exit flowfields and 2) the momentum change in the propellant. The mathematical relationships utilized to compute these ratios and fractions are not shown, but graphical results are illustrated in the Results Section of this thesis for specific operating conditions.

To further illustrate the performance of the ramjets operating with a perfect gas propellant it is instructive to express the first law of thermodynamics in the form

$$\frac{V_7}{V_1} = \left(\frac{T_{T_7}}{T_{T_1}}\right)^{\frac{1}{2}} \left\{ \frac{2}{M_1^2(\gamma-1)} \left[1 - \left(\frac{P_{T_7}}{P_{T_1}} \frac{P_1}{P_7}\right)^{\frac{1-\gamma}{\gamma}} \right] + 1 \right\}^{\frac{1}{2}} \tag{4}$$

and the momentum equation in the form

$$\frac{F}{\dot{m}V_1} = \left(\frac{V_7}{V_1} - 1\right) + \frac{1}{M_1^2\gamma} \left\{ \frac{T_{T_7}}{T_{T_1}} \left(\frac{P_{T_7}}{P_{T_1}} \frac{P_1}{P_7}\right)^{\frac{1-\gamma}{\gamma}} \frac{1}{(V_7/V_1)} - 1 \right\} . \tag{5}$$

Equation 5 can be multiplied by the quantity

$$\frac{V_1{}^2}{\frac{\gamma}{\gamma-1} R\, T_{T_1}\left(\frac{T_{T_7}}{T_{T_1}}-1\right)} \tag{6}$$

to obtain the form

$$\frac{FV_1}{\dot{Q}} = \frac{(\gamma-1)M_1^2}{\left(1+\frac{\gamma-1}{2}M_1^2\right)\left(\frac{T_{T_7}}{T_{T_1}}-1\right)}\left\{\left(\frac{V_7}{V_1}-1\right)+\frac{1}{M_1^2\gamma}\left[\frac{T_{T_7}}{T_{T_1}}\left(\frac{P_{T_7}}{P_{T_1}}\frac{P_1}{P_7}\right)^{\frac{1-\gamma}{\gamma}}\frac{1}{(V_7/V_1)}-1\right]\right\} \tag{7}$$

For the conventional ramjet

$$P_7/P_1 = 1. \qquad \text{not necessarily al supersonic exhaust}$$

The stagnation pressure ratio P_{T_7}/P_{T_1} is given by

$$\frac{P_{T_7}}{P_{T_1}} = \frac{P_{T_4}}{P_{T_1}}\frac{P_{T_5}}{P_{T_4}}\frac{P_{T_7}}{P_{T_5}}$$

where P_{T_4}/P_{T_1} is fixed by the inlet flow conditions and the diffuser geometry and P_{T_7}/P_{T_5} is unity. The stagnation pressure ratio P_{T_5}/P_{T_4} is dictated by the rate of heat addition per unit mass to the propellant and for subsonic heat addition this ratio does not vary appreciably. Examination of Eq. 4 shows that for fixed values of M_1, γ, P_{T_4}/P_{T_1}, P_1/P_7 and P_{T_7}/P_{T_5}, the effect of the variation of P_{T_5}/P_{T_4} on the expression

$$\left\{\frac{2}{M_1^2(\gamma-1)}\left[1-\left(\frac{P_{T_7}}{P_{T_1}}\frac{P_1}{P_7}\right)^{\frac{1-\gamma}{\gamma}}\right]+1\right\}^{\frac{1}{2}}$$

is small compared to the change in

$$\left(\frac{T_{T_7}}{T_{T_1}}\right)^{\frac{1}{2}}$$

as the rate of heat addition per unit mass is varied. As a result, Eq. 4 can be written

$$\frac{V_7}{V_1} \cong K_1 \left(\frac{T_{T_7}}{T_{T_1}}\right)^{\frac{1}{2}} \tag{8}$$

where K_1 is approximately constant. The variation in K_1 is typically of the order of 5% for the cases considered.

Optimum Ramjet Operation

It will be shown in the Results Section of this thesis that there is a value of the non-dimensional thrust $[F/P_1 A_1]$ for which the instantaneous thermal efficiency $[FV_1/\dot{Q}]$ is at a maximum for a specified diffuser and given free-flow inlet conditions. An approximate mathematical relationship which predicts the point of maximum efficiency for the conventional ramjet operating with a perfect gas propellant can be derived by considering the first law of thermodynamics and the momentum equation. The quantity appearing in Eq. 5

$$\left(\frac{P_{T_7}}{P_{T_1}} \frac{P_1}{P_7}\right)^{\frac{1-\gamma}{\gamma}}$$

varies by about 6.5% at the most, so it can be treated as a constant. By assuming that the previously mentioned quantities are constant Eq. 5 can be put into the following functional form

$$\frac{F}{\dot{m}V_1} \doteq A\left(\frac{T_{T_7}}{T_{T_1}}\right)^{\frac{1}{2}} - B \tag{9}$$

where A and B are constants. This equation states that the ramjet thrust varies as the square root of the heat addition rate per unit mass. Similarly the expression for instantaneous efficiency (Eq. 7) can be put into the form

$$\frac{FV_1}{\dot{Q}} \doteq \frac{C\left(\frac{T_{T_7}}{T_{T_1}}\right)^{\frac{1}{2}} - D}{\frac{T_{T_7}}{T_{T_1}} - 1} \tag{10}$$

where C and D are constants.

Examination of Eq. 10 reveals that there is an optimum stagnation temperature ratio that will yield a maximum instantaneous efficiency. From Eq. 9 one sees that this optimum temperature ratio corresponds to an optimum normalized thrust level. This optimum corresponds to a ramjet characterized by specified geometry and inlet conditions. Changes in the inlet condition will necessitate changes in the optimum stagnation temperature ratio and the optimum normalized thrust level. The values for the constants C and D are given by

$$C = K_2(K_1 + K_3 K_4)$$

$$D = K_2(1 + K_3)$$

where

$$K_1 = \left\{\frac{2}{M_1^2(\gamma-1)}\left[1 - \left(\frac{P_{T_7}}{P_{T_1}}\frac{P_1}{P_7}\right)^{\frac{1-\gamma}{\gamma}}\right] + 1\right\}^{\frac{1}{2}}$$

$$K_2 = \frac{(\gamma-1)M_1^2}{(1+\frac{\gamma-1}{2}M_1^2)}$$

$$K_3 = \frac{1}{M_1^2 \gamma}$$

$$K_4 = \frac{\left[(P_{T_7}/P_{T_1})(P_1/P_7) \right]^{\frac{1-\gamma}{\gamma}}}{K_1}$$

These relations are valid where P_1/P_7 is held to be constant and the stagnation pressure ratio P_{T_5}/P_{T_4} takes on typical values in the range 0.8 to 1.0. By differentiating the instantaneous efficiency (Eq. 10) with respect to the stagnation temperature ratio, the stagnation temperature ratio which gives the optimum instantaneous efficiency can be computed. The expression for this optimum ratio is

$$\left(\frac{T_{T_7}}{T_{T_1}} \right)_{\frac{FV_1}{\dot{Q}} = \text{Maximum}} = \left\{ \frac{D}{C} + \left(\frac{D^2}{C^2} - 1 \right)^{\frac{1}{2}} \right\}^2 . \tag{11}$$

Dissociating Flow Model

It was anticipated that assuming the propellant behaves as a perfect gas would introduce errors into these analyses, because it was recognized that effects such as vibrational and electronic excitation dissociation and ionization of the propellant would play significant roles in the performance of the ramjet device. The annular flow electrothermal plug ramjet was also analyzed with the above effects included. The validity of assuming either chemically frozen or equilibrium chemical composition in the supersonic nozzle expansion was also evaluated. In analyzing the flow in the diffuser for this dissociating flow case it was assumed that the fluid in the conical flowfield between the normal

shock and the oblique shock behaved as a perfect gas and thus that this portion of the model developed for the perfect gas models could be applied. This assumption should not introduce too much error into this analysis because the oblique shock angle should be shallow for high inlet velocities and small diffuser cone angles, and the temperature rise in the conical flowfield should not be too large. Downstream of the normal shock, chemical relaxation and other non-perfect gas modes of energy storage were allowed to occur in the propellant. The propellant was assumed to be in thermodynamic equilibrium downstream of the normal shock and up to the annular nozzle throat (6). Finite chemical reaction rates were evaluated in the supersonic nozzle expansion between 6 and 7. Because shifting chemical equilibrium was allowed, closed form equations for the thermodynamic properties could not be obtained. The method of analysis utilized for the model including shifting composition involved piece-wise application of the momentum and energy equations between each state identified in Fig. 3b that is downstream of the normal shock.

In order to compare the performance of the perfect gas ramjet to that of the ramjet utilizing the chemically reacting propellant, the diffuser operating conditions are specified and the non-dimensional thrust is computed along with various other non-dimensional parameters such as the inlet/exit temperature and velocity ratios. Different values for the non-dimensional thrust $[F/P_1A_1]$ are determined by independently varying each component in the non-dimensional thrust equation, and the downstream flow conditions are found such that a specified, constant thrust level is met.

RESULTS

It is instructive to examine a ramjet operating at a typical
flight velocity that would be encountered at one point in a launch se-
quence so that the influences of the various operational parameters
can be established. In order to do this several different ramjet con-
figurations have been analyzed for a moderate flight velocity of
7000 m/s. A diffuser cone half-angle (δ) of 30°, a static temperature
(T_1) of 300°K, and diffuser shoulder diameter-to-tube diameter (d_3/d_1)
and heat addition region diameter-to-tube diameter (d_4/d_1) ratios of
0.805 and 0.403 respectively (Fig. 3), have been used in the analysis.
The 30° cone angle assured conical shock attachment and reasonable diffuser
efficiency. The static temperature T_1 was selected as a reasonable
value that could exist in an actual device. The diameter ratios re-
sulted in adequate center body structural integrity and they were also
such that choking at the diffuser throat was precluded. The specific
ramjet configurations examined are (1) the conventional ramjet utilizing
diatomic hydrogen which behaves as a perfect gas as a working fluid and
with the constraint that the inlet and outlet static pressures are equal,
(2) the annular flow electrothermal ramjet operating with the same per-
fect gas and with the constraint that the inlet and outlet flow areas
are equal and (3) the annular flow electrothermal ramjet operating with
hydrogen propellant that is allowed to dissociate and ionize and to have
vibrational and electronic modes of energy storage along with finite

chemical relaxation rates occurring in the supersonic nozzle expansion. For this latter case two thrust levels per unit cross sectional area of tube have been specified. The higher value for the thrust per unit area is $F/A_1 = 9.5 \times 10^7$ Pa and the lower value for the thrust per unit area is $F/A_1 = 9.5 \times 10^6$ Pa. Two values have been considered so that the effect of varying the initial pressure in the launch tube can be illustrated for high and low thrust per unit area values.

Figure 4 illustrates the relationship between the instantaneous efficiency $[FV_1/\dot{Q}]$ and the non-dimensional thrust $[F/P_1A_1]$ for the previously mentioned operational parameters. Increasing the non-dimensional thrust implies increasing the heat addition per unit mass to the propellant. The perfect gas conventional ramjet is shown to exhibit the best performance, and the optimum value for instantaneous efficiency is seen to occur at a non-dimensional thrust of 12 for the conventional ramjet. This peak value is predicted to first order by Eq. 10.

The consequence of not expanding the supersonic nozzle flow to the pressure ratio P_7/P_1 of unity is illustrated in Fig. 4 by the curve for the electrothermal plug ramjet operating with a perfect gas (no dissociation). Its performance is seen to be degraded substantially with respect to the conventional ramjet operating with a perfect gas. The other curves, which illustrate the effects of chemical freezing, dissociation, ionization and vibrational and electronic modes of energy storage, are shown to exhibit performance which is similar but inferior to the electrothermal plug ramjet operating with a perfect gas. It is noted that the dissociating propellant curves of Fig. 4 were generated by fixing the thrust-to-cross sectional area ratio (F/A_1) and varying the initial pressure in the launch tube P_1. The maximum value of the
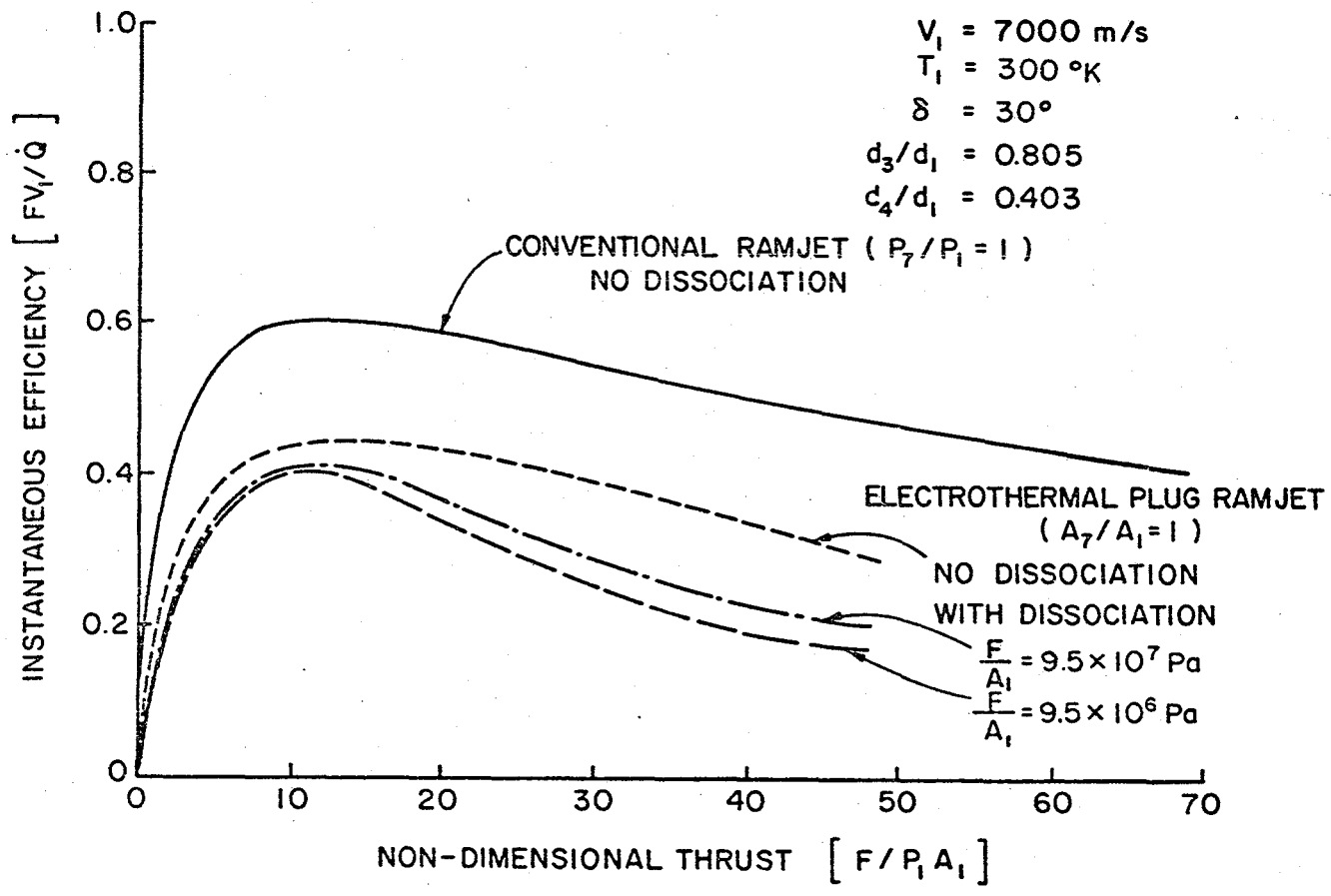
Fig. 4 Instantaneous Efficiency Profiles

non-dimensional thrust for which each curve shown in Fig. 4 terminates is that value for which no more hea: could be added in the heat addition region of the respective ramjets without choking the flow at the exit of the heat addition region 5. All of the curves in Fig. 4 illustrate, that for a given velocity and diffuser geometry, there is a value for the non-dimensional thrust which provides the maximum instantaneous efficiency. It is also evident that, for the case of a dissociating propellant, a high tube pressure high thrust device corresponding to the higher thrust per unit area (F/A_1 = 9.5 x 10^7 Pa) provides performance superior to a low tube pressure low thrust device (F/A_1 = 9.5 x 10^6 Pa). This is due to the greater level of dissociation that occurs at the lower pressures. Figure 5 illustrates this by showing that the mass fraction of diatomic hydrogen in the ramjet exhaust is greater at the higher thrust per unit area level where the initial tube pressure is higher at a given non-dimensional thrust. It is evident that high values of the non-dimensional thrust can be achieved before dissociation becomes important and that increasing the initial tube pressure P_1 decreases the amount of dissociation in the propellant.

Figure 6 shows the effect of non-dimensional thrust on the fraction of the total thrust that is produced by the differential pressure-area product across the ramjet. The conventional ramjet operating with a perfect gas derives a smaller fraction of thrust from the pressure-area differential than the other ramjet configurations. The electrothermal plug ramjet operating with a perfect gas obtains a greater fraction of thrust from the differential of the pressure area product than the conventional ramjet for a given value of the non-dimensional thrust. The
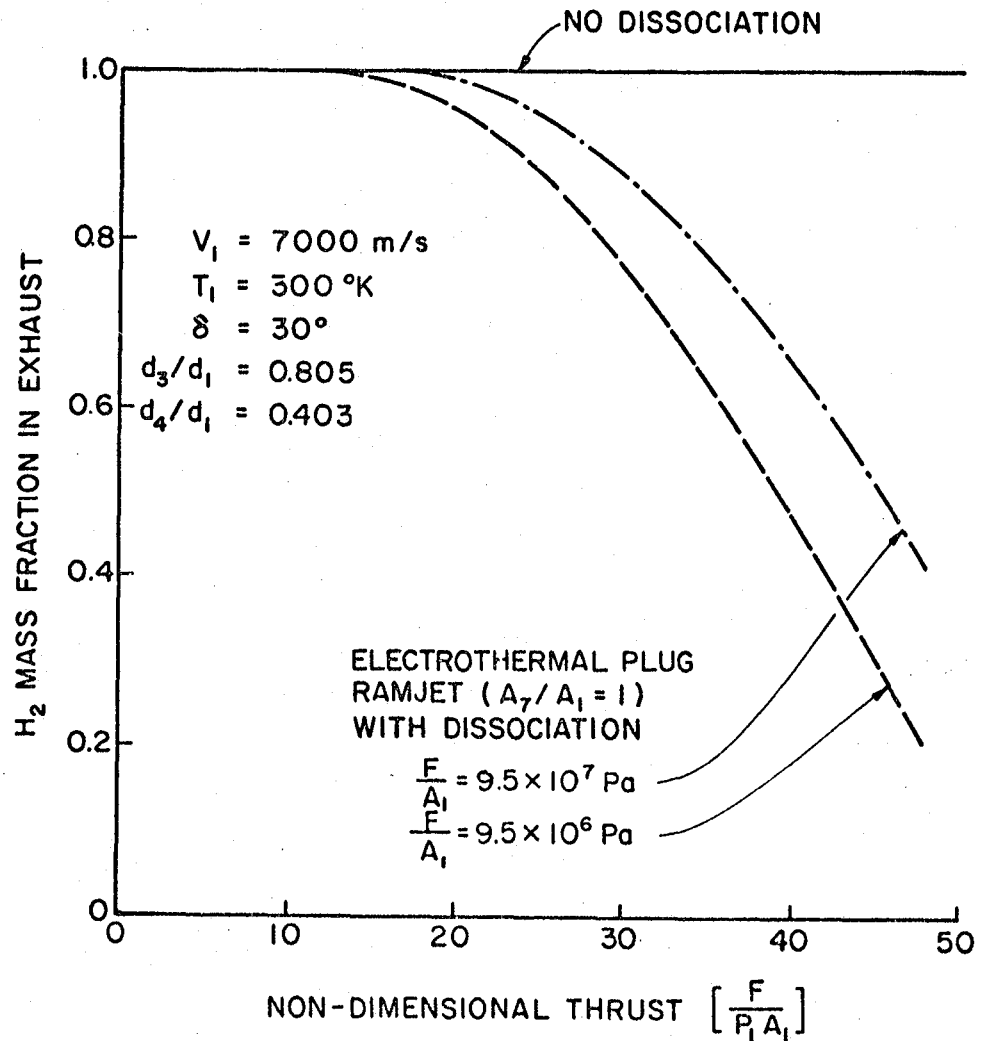
Fig. 5 Mass Fraction of H_2 in Exhaust
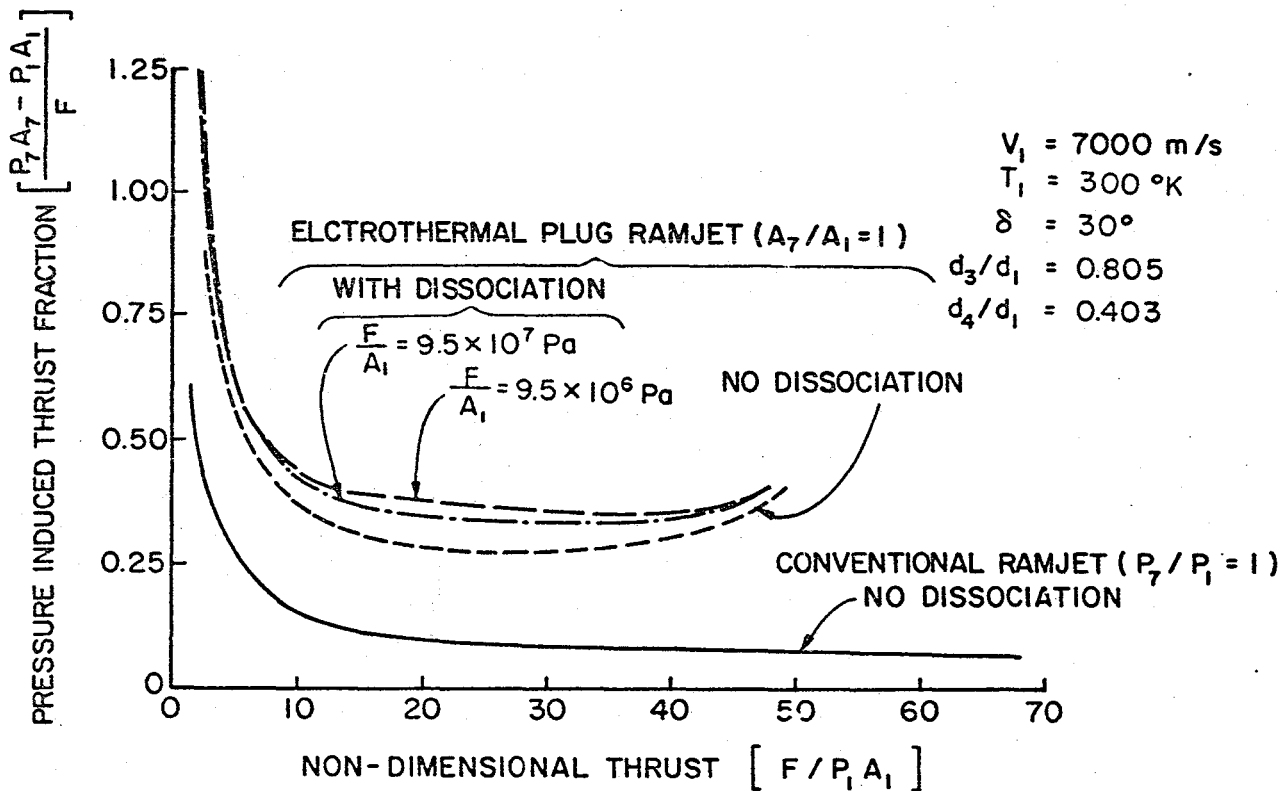
Fig. 6 Pressure-Induced Thrust
Fraction Profiles

electrothermal ramjet analyses which consider non-perfect gas effects show that including these effects causes the pressure induced thrust fraction to rise over that given for the perfect gas, electrothermal ramjet. The high tube pressure, high thrust ramjet operates with a lower pressure-induced thrust fraction than the low tube pressure, low thrust ramjet.

Figure 7 illustrates the relationship between the exit/inlet static pressure ratio and the non-dimensional thrust for the different ramjet models considered. By design, the exit/inlet pressure ratio is unity for the conventional ramjet. The electrothermal plug ramjet operating with a perfect gas exhibits lower pressure ratios than the electrothermal plug ramjet operating with a reacting propellant. For the electrothermal plug ramjet operating with a reacting propellant, high thrust, high pressure operation is seen to exhibit slightly lower exit/inlet pressure ratios than low thrust, low pressure operation.

The exit/inlet velocity ratios for the different ramjet configurations are shown in Fig. 8. The conventional ramjet exhibits a nearly linear dependence between the exit/inlet velocity ratio and the non-dimensional thrust. It has been suggested previously that, for a conventional ramjet, both the thrust (Eq. 9) and the exit/inlet velocity ratio (Eq. 8) show rates of change approximately proportional to the square root of the total temperature ratio (T_{T_7}/T_{T_1}), so a linear dependency between the thrust and the exit/inlet velocity ratio is to be expected. The results obtained for the electrothermal plug ramjet operating with a perfect gas show that the velocity ratio is degraded with respect to the conventional ramjet. This curve is not linear because the outlet/inlet static pressure ratio increases with
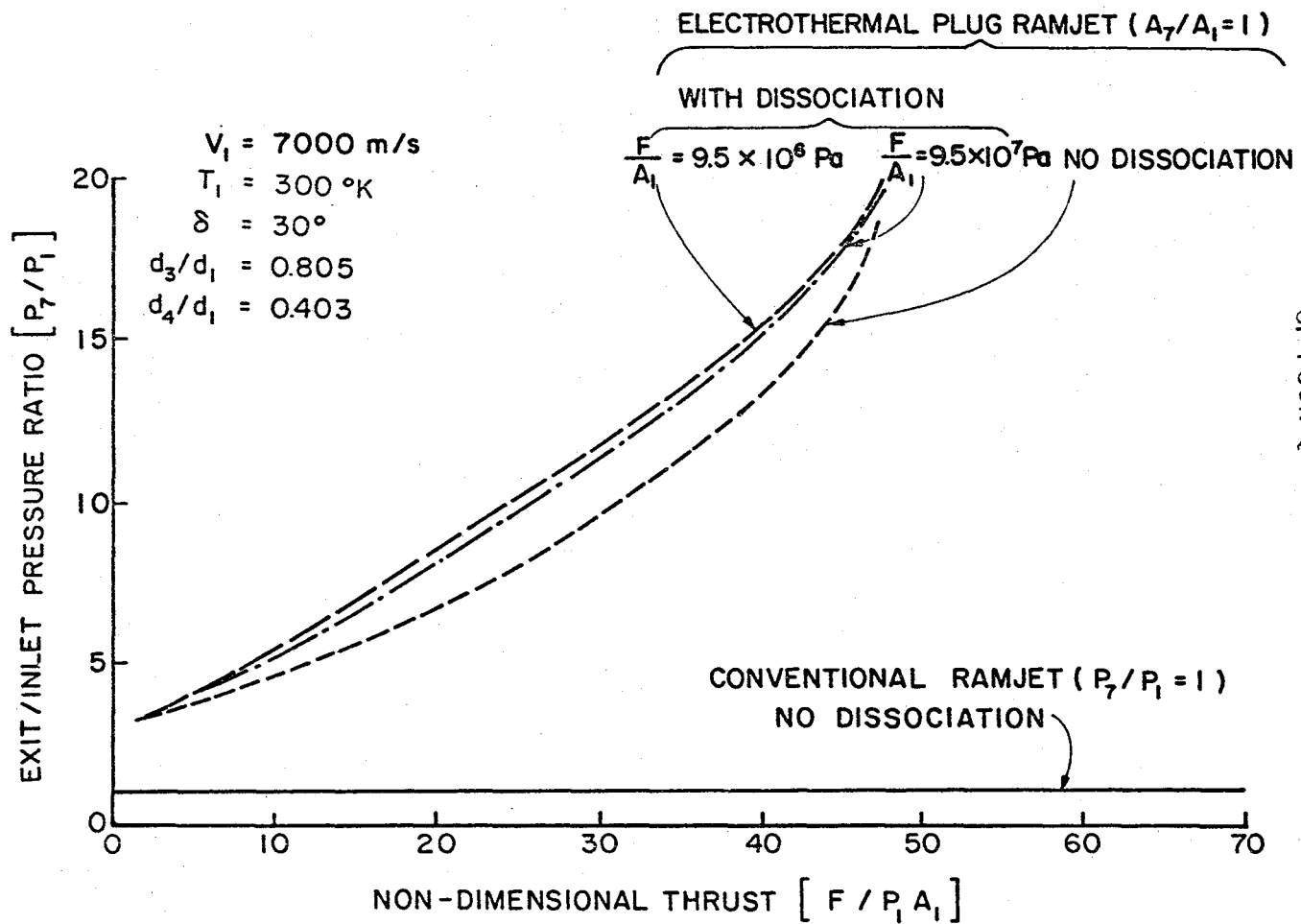
Fig. 7   Outlet/Inlet Pressure Ratio Profiles

ELECTROTHERMAL PLUG RAMJET ($A_7/A_1 = 1$)

WITH DISSOCIATION

$\dfrac{F}{A_1} = 9.5 \times 10^6$ Pa $\dfrac{F}{A_1} = 9.5 \times 10^7$ Pa NO DISSOCIATION

$V_1 = 7000$ m/s
$T_1 = 300\,°K$
$\delta = 30°$
$d_3/d_1 = 0.805$
$d_4/d_1 = 0.403$

CONVENTIONAL RAMJET ($P_7/P_1 = 1$)
NO DISSOCIATION

EXIT/INLET PRESSURE RATIO $\left[P_7/P_1 \right]$

NON-DIMENSIONAL THRUST $\left[F / P_1 A_1 \right]$
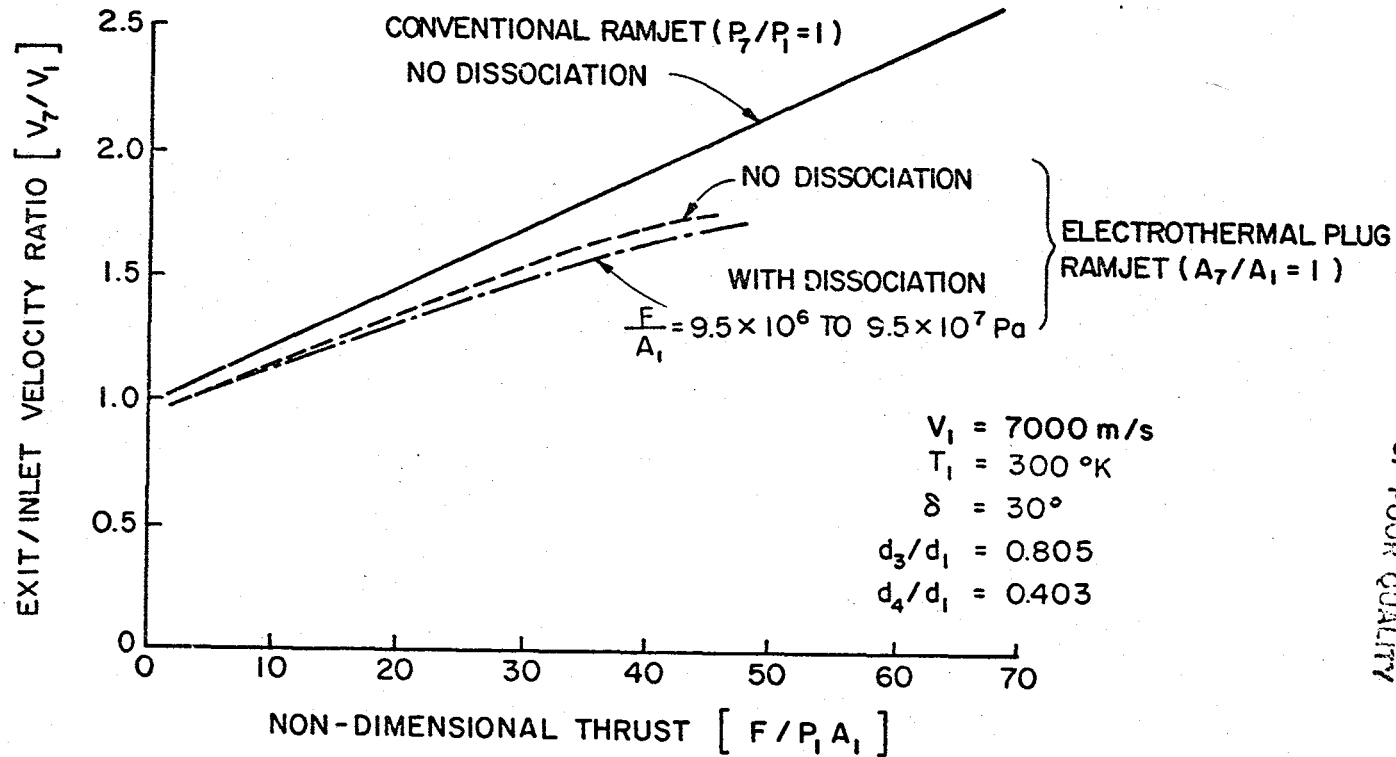
Fig. 8 Outlet/Inlet Velocity Ratio Profiles

non-dimensional thrust for the plug ramjet (a nearly constant static

pressure ratio is essential to ensure linearity, as described by

Eqs. 4 and 5). The electrothermal plug ramjet results including dis-

sociation demonstrate that the exit/inlet velocity ratio is degraded

with respect to the perfect gas configurations. Only one curve is

shown for the cases including dissociation. This is because the data

for the two different cases were very close, and a true distinction

was difficult to show graphically. The actual data indicate that the

high thrust high pressure device operates with a slightly greater velo-

city ratio than the low thrust, low pressure device. This degradation

in the momentum change of the propellant between the inlet and outlet

is offset by greater exit/inlet pressure ratios so that desired thrust

levels can be achieved. Figure 8 also brings to light the fact that

the exit/inlet velocity ratio can be less than unity. This implies a

momentum change of the propellant detracts from the thrust and requires

that the differential pressure-area product must supply more thrust.

In Fig. 6, these regions of operation where the pressure-induced thrust

fraction is greater than unity are observed at the low normalized

thrusts where the velocity ratio V_7/V_1 is less than unity. These regions

also correspond to the low efficiency regions illustrated in Fig. 4.

In Fig. 9 the relationship between the exit/inlet temperature ratio

and the non-dimensional thrust is illustrated for the different ramjet

configurations. The conventional ramjet exhibits a lower temperature

ratio than the other ramjet configurations because of the more complete

nozzle expansion. In the case of the electrothermal plug ramjet, the

dissociating propellant cases are shown initially to exhibit greater

temperature ratios than the electrothermal plug ramjet operating with a

perfect gas, and the temperature ratios for the dissociating propellant
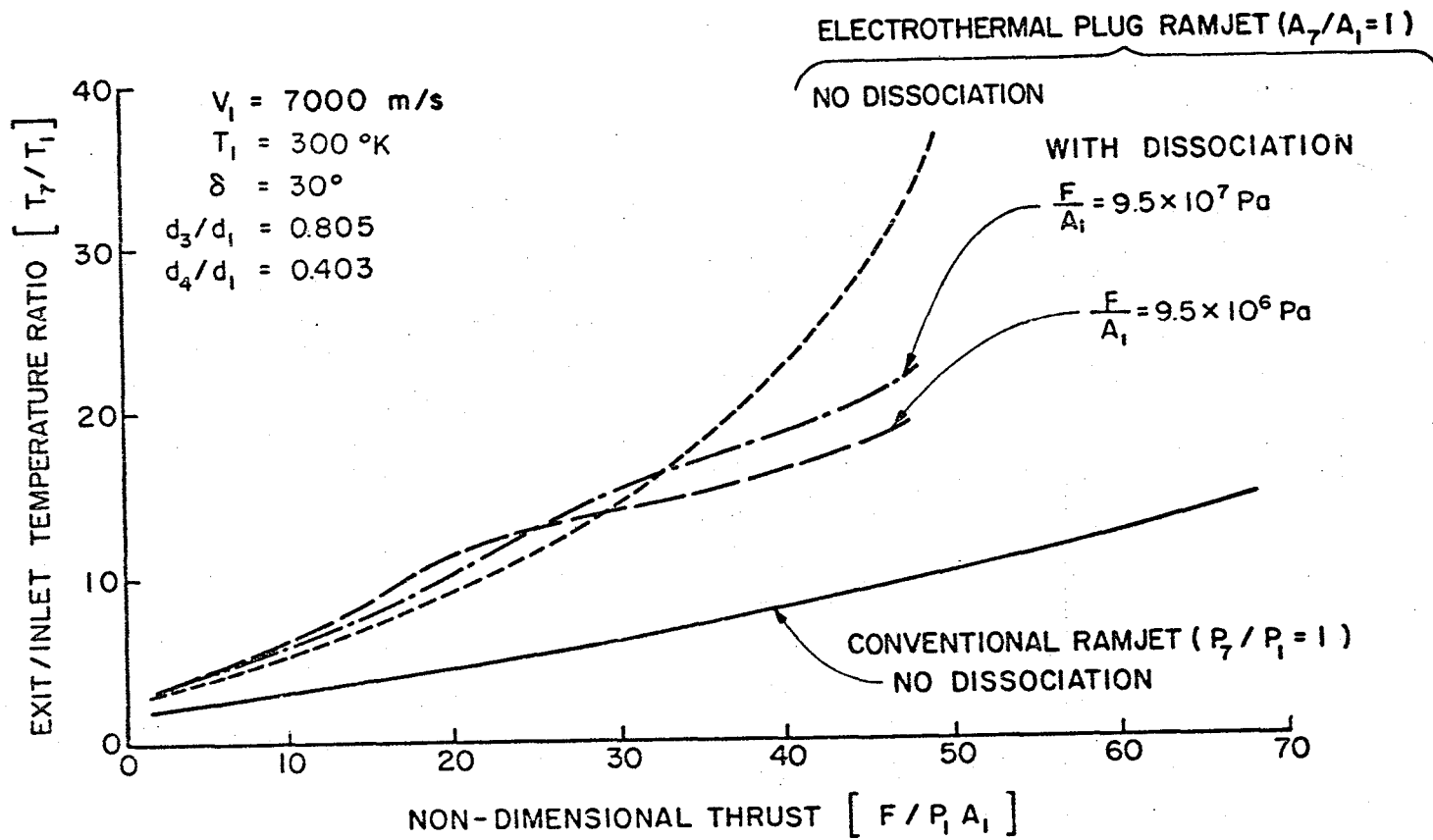
Fig. 9 Outlet/Inlet Static Temperature Profiles

drop below those shown for the perfect gas electrothermal plug ramjet
as the non-dimensional thrust is increased. This lowering of the exit/
inlet temperature ratio is due to the dissociation of the propellant.

The effect of changes in the flight velocity on the instantaneous
efficiency can be seen by comparing the results of Fig. 4 (V_1 = 7,000 m/s)
with those of Figs. 10 (V_1 = 15,000 m/sec) and Fig. 11 (V_1 = 4,000 m/sec).
All of the other operational parameters mentioned previously, such as
the diffuser cone half-angle, are the same as for the 7,000 m/s flight
velocity, except for the diameter ratios d_3/d_1 and d_4/d_1. The diam-
eter ratio d_3/d_4 = 2 has been specified to be constant for any velocity.
As the ramjet flight velocity increases, the conical shock angle will
decrease if the conical diffuser half-angle is held constant. Because
it has previously been specified that the intersection of the oblique
shock and the tube wall occurs at the diffuser shoulder, the tube diam-
eter must decrease as the projectile velocity increases for a constant
ramjet annular diffuser geometry. This is why the diameter ratios d_2/d_1
and d_4/d_1 increase as the flight velocity increases. Examining Figs. 10
and 11 one sees that the same trends associated with the 7000 m/s
results are evident in these figures (i.e., there is a value of the
non-dimensional thrust for which the instantaneous efficiency is
optimized). A very important feature of ramjet operation is brought
out by examining Figs. 4, 10 and 11. This feature is that in order for
ramjet operation to remain at a reasonable efficiency level during ac-
celeration, the non-dimensional thrust must vary greatly over the
region of acceleration. Assuming that a constant thrust level (F) is
desired and that the inlet area (A_1) does not change appreciably during
the launch of a given plug projectile makes it apparent that the static
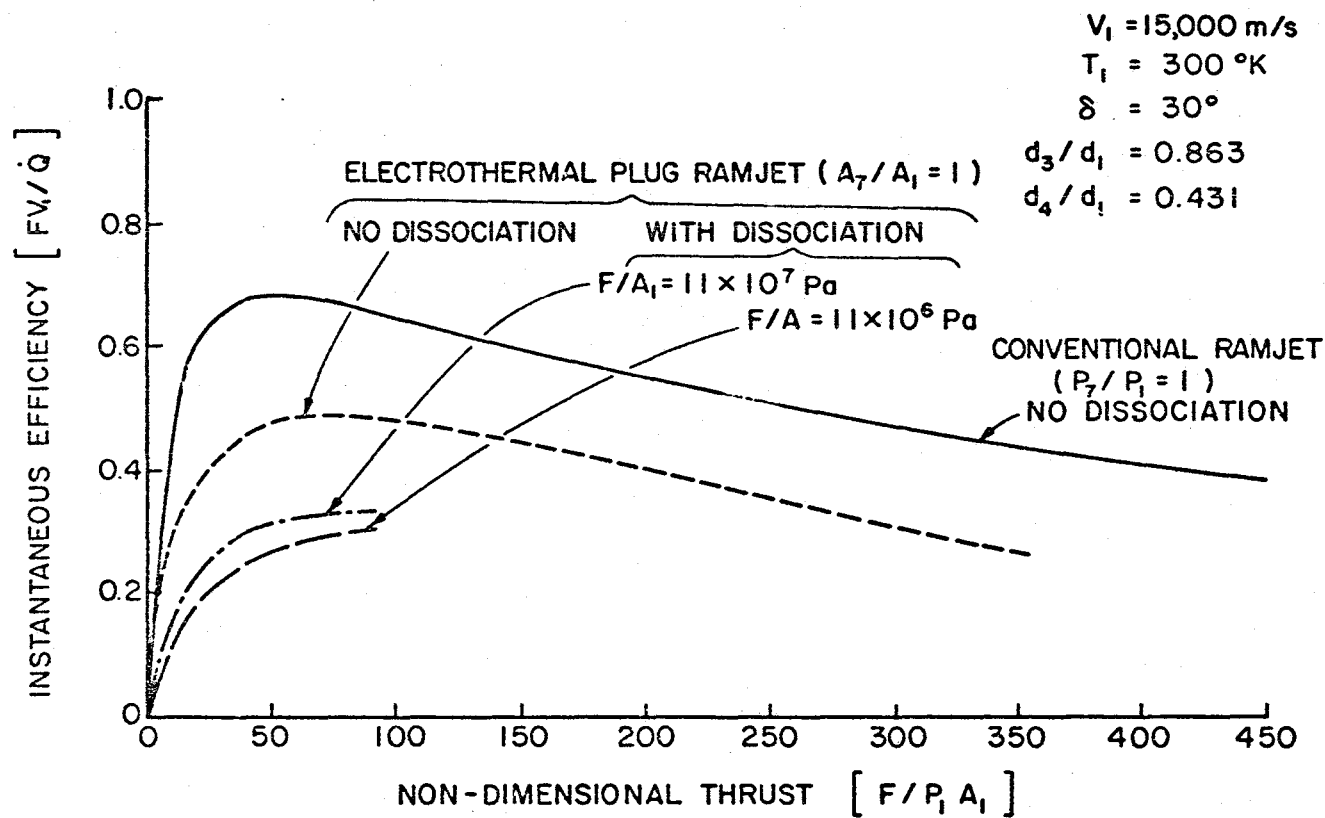
Fig. 10   Instantaneous Efficiency Profiles
at High Velocity
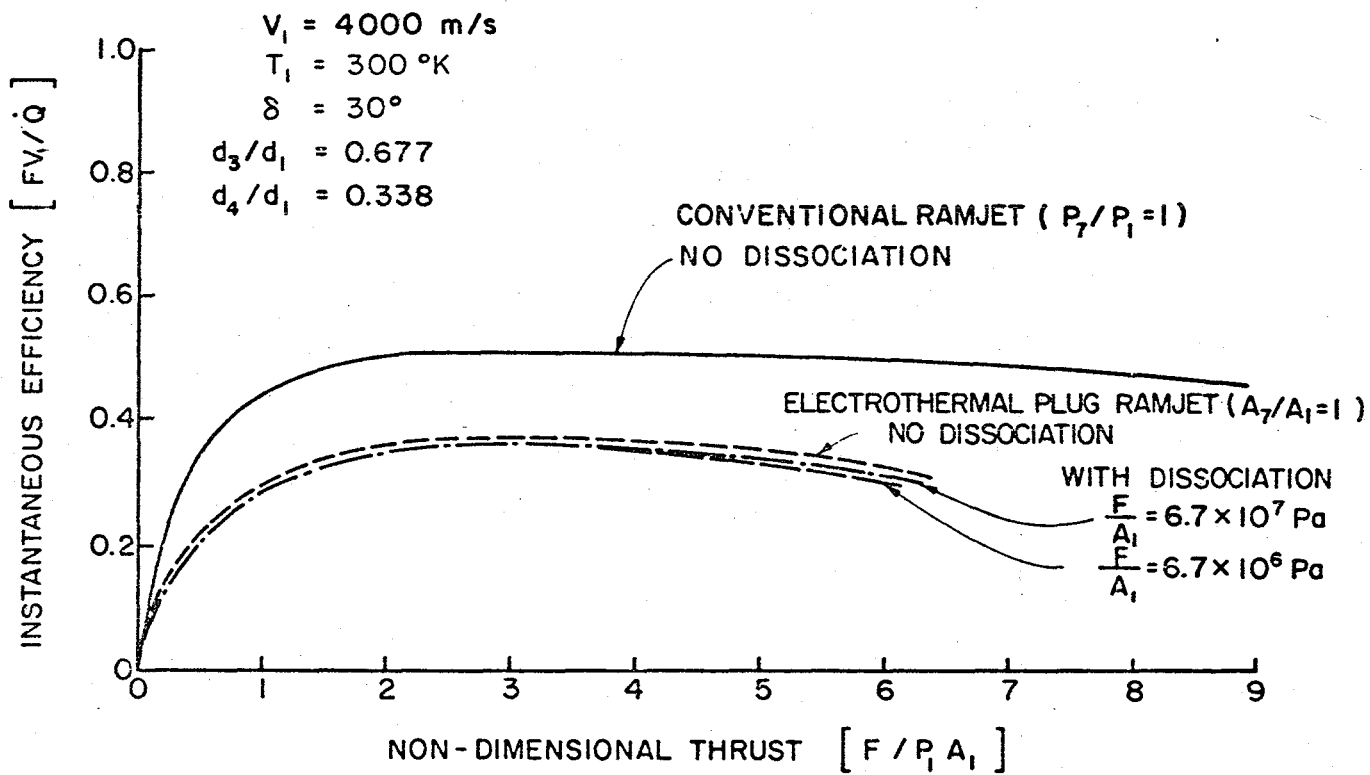
Fig. 11 Instantaneous Efficiency Profiles
at Low Velocity

propellant pressure immediately upstream of the ramjet must decrease as the ramjet velocity increases so that efficient operation can be maintained. It is noted that the data in Fig. 10 for the dissociating propellant, electrothermal plug ramjet are terminated at a value of 90 for the non-dimensional thrust because ionization of the propellant started to become significant past this value.

The results of Fig. 12 were obtained from a series of plots like those in Figs. 4, 10 and 11. They illustrate the variation in the non-dimensional thrust which must be achieved to attain the maximum instantaneous efficiency over a velocity range of 4,000 m/s to 15,000 m/s. The non-dimensional thrust is observed to vary from a minimum of 4 at 4,000 m/s to a maximum of around 50 for a velocity of 15,000 m/s. These results are for the dissociating propellant.

Figure 13 illustrates the maximum instantaneous efficiency attainable for a mission where a projectile is accelerated from 4,000 m/s to 15,000 m/s utilizing two different thrust levels. The operational parameters are the same as previously defined. To attain the performance shown in Figure 13 the non-dimensional thrust must follow the non-dimensionalized thrust profile given in Fig. 12. This means that P_1 must be varied continuously along the launch tube. For high velocities, the high thrust profile exhibits performance superior to the low thrust profile because high static tube pressures are associated with high thrust operation, and propellant dissociation is less significant for the high pressure case than for the low pressure case. The optimum value for the instantaneous efficiency is observed to be near 7,000 m/s because this is the velocity for which this particular diffuser

$T_1 = 300\,°K$
$\delta = 30°$

RAMJET VELOCITY (km/sec)

EFFICIENCY $\left[F/P_1 A_1 \right]$

NON-DIMENSIONAL THRUST AT MAXIMUM
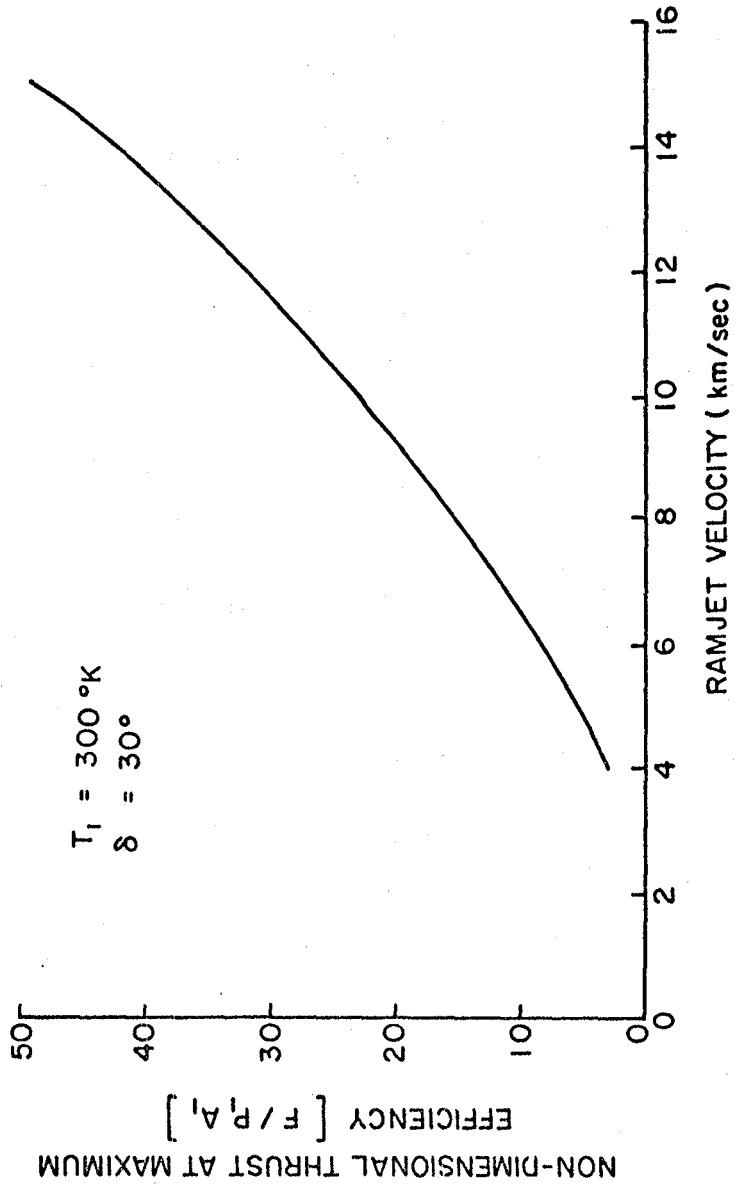
Fig. 12 Non-Dimensional Thrust Profile
for Maximum Efficiency
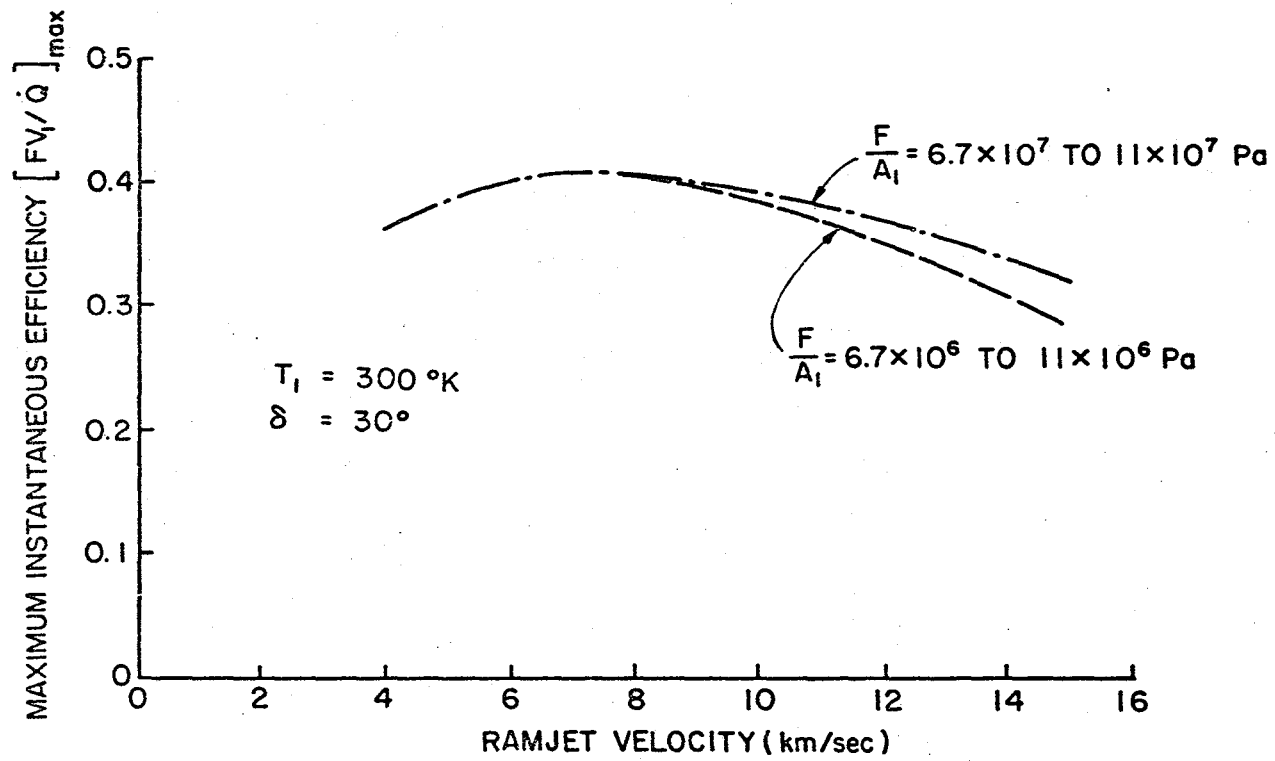
Fig. 13 Maximum Instantaneous Efficiency Profiles

performs the best. Changing the diffuser geometry will change the location of the optimum point.

Several profiles are shown in Fig. 14 which detail the performance of a ramjet as it accelerates 10 kg at a level of 30,000 g's. These profiles were computed for various conical diffuser half-angles and for tube static pressures that remain at fixed values along the tube length. For purposes of comparison, the optimum efficiency performance data for the high thrust per unit area values given earlier are plotted with the results obtained for constant tube pressure acceleration. These values of the thrust per unit area coupled with the specified projectile mass produces an acceleration of 30,000 g's. The early portions of the curves where no data are shown are those portions of the launches where the ramjet propulsion system could not achieve the specified thrust and where light gas gun induced acceleration would be used. The influence of the tube pressure can be clearly seen by comparing the results for tube pressures (P_1) of 30 and 60 atmospheres and for a conical half-angle of 30°. Early in the operation, a high tube pressure is shown to exhibit superior performance, while towards the end of the acceleration period the lower tube pressure exhibits the superior performance. The results plotted for the optimum performance suggest that the variation in tube pressure is important in order to maintain high efficiency.

The effect of varying the conical diffuser half-angle is also illustrated in Fig. 14. Having a diffuser cone half-angle that is either too shallow or too steep degrades the performance. For the missions analyzed in this paper, the overall optimum conical half-angle was near 30°.

$\triangledown$ δ = 30°   P VARIED FOR OPTIMUM
                                        PERFORMANCE

○ δ = 30° P_I = 60 atm
□ δ = 45° P_I = 30 atm
△ δ = 10° P_I = 30 atm
◇ δ = 30° P_I = 30 atm

σ = 30,000 g's
T_I = 300 °K
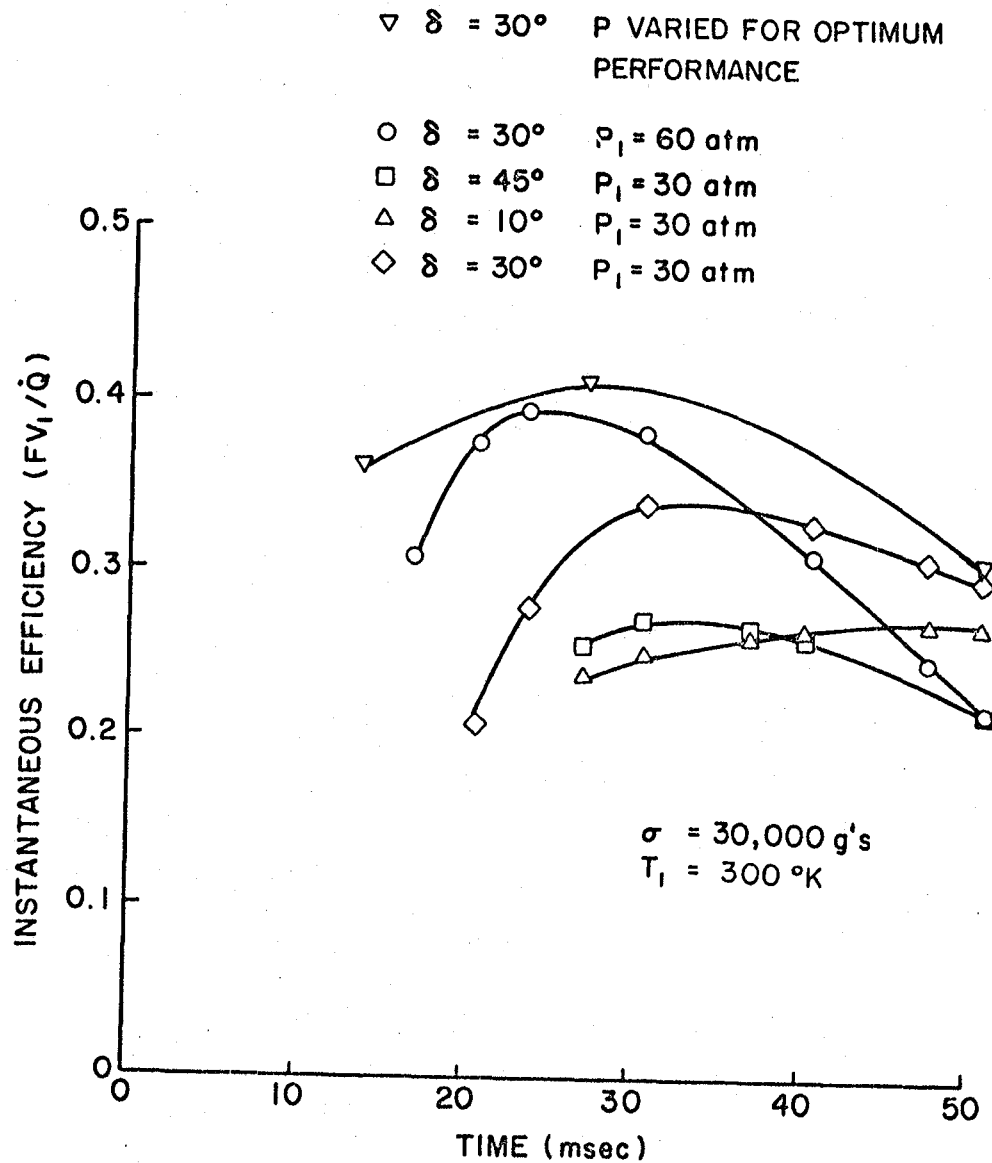
Fig. 14 Efficiency Profiles over Typical Launch Cycles

By applying the first law of thermodynamics and the momentum equation to the control volume shown in Fig. 3b, expressions for the non-dimensional thrust and the instantaneous efficiency can be put in the following forms respectively

$$\frac{F}{P_1 A_1} = \frac{\rho_1 V_1^2 (V_7/V_1 - 1) + P_1(P_7/P_1 - 1)}{P_1} \qquad (12)$$

$$\frac{F V_1}{\dot{Q}} = \frac{\rho_1 V_1^2 (V_7/V_1 - 1) + P_1(P_7/P_1 - 1)}{\rho_1 q} \cdot \qquad (13)$$

Examination of Eqs. 12 and 13 illustrates that for given constant inlet conditions the non-dimensional thrust and the instantaneous efficiency will remain constant if the heat addition per unit mass (q), the exit/inlet velocity ratio (V_7/V_1) and the exit/inlet pressure ratio (P_7/P_1) remain constant. In order for these parameters to remain constant it is required that the propellant thermodynamic properties remain constant throughout the ramjet flowfield shown in Fig. 3b. To ensure a consistent solution for the flowfield at state 4 shown in Fig. 3b, it is necessary to keep the diameter ratio d_1/d_4 and the conical diffuser half-angle (δ) constant for whatever flight velocity is being considered. Keeping these variables constant allows the results given here to be scaled for different size projectiles and thrust levels.

CONCLUSIONS

The results presented in this thesis have extended the results obtained from earlier analyses.[1] The earlier analyses assumed isentropic diffuser operation and perfect gas propellant behavior, while the present analysis takes into account such effects as diffuser shock losses, dissociation and ionization of hydrogen propellant, and nonequilibrium processes in the supersonic nozzle expansion. It has been demonstrated that diffuser losses, while significant, do not degrade ramjet performance to unacceptably low levels. The diffuser geometry does affect performance significantly if the diffuser conical half-angle is too shallow or too steep. At the overall optimum conical half-angle for the cases presented here ($\sim 30°$) however the performance degradation is not excessive.

In the analyses conducted in this thesis, it has been assumed that the propellant is in thermodynamic equilibrium up to the throat of the annular nozzle, and nonequilibrium processes are allowed to occur in the supersonic nozzle expansion downstream of the nozzle throat. Chemical nonequilibrium in the nozzle expansion was evaluated, and it was found that the nozzle flowfield was typically found to be very near chemical equilibrium. Because chemical relaxation times are generally larger than other nonequilibrium process relaxation times (such as vibrational, translational and rotational processes) the assumption that the propellant is in thermodynamic equilibrium should not introduce significant errors into the analyses.

It has been demonstrated that the static propellant pressure immediately upstream of the electrothermal ramjet affects performance significantly. Changing this pressure effectively changes the mass flow rate and the rate of heat addition per unit mass and it is demonstrated that for a particular flight velocity there is an optimum rate of heat addition per unit mass. When dissociation and ionization are allowed to occur, it is shown that decreasing the static propellant pressure increases the losses due to dissociation and ionization. However, the results presented demonstrate that it is feasible to operate in operational regimes where dissociation and ionization do not significantly degrade ramjet performance. To maintain peak efficiency the static propellant pressure immediately ahead of the ramjet must decrease as ramjet velocity increases.

The assumption of quasi-steady fluid flow used in this analysis will surely introduce some error. It is possible that the mass of the propellant contained within the ramjet could change, and the fact that the propellant within the ramjet is also accelerating could also introduce significant errors. The acceleration could cause a "hydrostatic" pressure difference to occur within the ramjet heat addition zone, which would possibly invalidate the results presented. An initial analysis of these effects has been conducted and is detailed in Appendix Γ. This analysis demonstrates that the non-steady gas dynamic effects just mentioned do not introduce errors which invalidate the results which are presented. The results from this analysis are based on calculations which compute flowfield changes over typical ramjet fluid particle residence times. Indeed, the idea is put forward that

proper tailoring of the upstream propellant conditions will minimize the unsteady gas dynamics effects to the point where they are not important.

Much analysis remains to be done to investigate completely the effects of all of the parameters of concern. The problems of projectile material selection and design have not been addressed nor have the details of the heat addition process been examined. It is possible that pressure oscillations could occur in a device of this type, and these oscillations will be related to the unsteady gas dynamics effects. Additional work related to maintenance of the correct projectile base pressure and static pressure immediately ahead of the projectile remains to be done. Although this aspect of the problem has not yet been studied, it intuitively seems possible that methods will be found which will allow for maintenance of the correct pressures. It is also possible that three-dimensional flow effects could become significant.

The results presented earlier have demonstrated that the conventional ramjet has the capability to outperform the plug ramjet. However, the mechanical complexities associated with conventional ramjet operation (such as providing efficient shock swallowing and producing the necessary nozzle conditions) are very significant. It is therefore argued that the plug ramjet, because of its apparent mechanical simplicity, is a more desirable device for effecting high acceleration launches.

The results presented suggest that the electrothermal ramjet concept cannot be rejected on the basis that it violates a basic principle of fluid mechanics or thermodynamics. Further, the results presented suggest that the electrothermal ramjet has the potential of accelerating payloads to high velocity with a good energy utilization

efficiency. For these reasons it is concluded that further analysis related to the design and development of the electrothermal ramjet concept is warranted.

REFERENCES

1. Wilbur, P. J., Mitchell, C. E. and Shaw, B. D., "The Electrothermal
      Ramjet," Journal of Spacecraft and Rockets, November-December
      1983, pp. 603-610.

2. Shaw, B. D., "The Electrothermal Ramjet," appears in "Advanced Ion
      Thruster and Electrothermal Launcher Research," P. J. Wilbur
      ed., NASA-CR-168083, Jan. 1983, pp. 36-48.

3. Mitchell, C. E., "Constant Pressure Acceleration of the Electro-
      thermal Ramjet," appears in "Advanced Ion Thruster and
      Electrothermal Launcher Research," P. J. Wilbur ed., NASA-CR-
      168083, Jan. 1983, pp. 49-71.

4. Lukasiewicz, J., Experimental Methods of Hypersonics, Marcel
      Dekker, Inc., 1973, pp. 95-101.

A1. Anderson, J. D., Modern Compressible Flow, McGraw-Hill, New York,
      1982, Chap. 10.

A2. Lukasiewicz, J., Experimental Methods of Hypersonics, Marcel
      Dekker, Inc., 1973, pp. 95-101.

B1. Bond, J. W., Watson, K. M., and Welch, J. A., Atomic Theory of Gas
      Dynamics, Addison-Wesley, Reading, MA, 1965, p. 85.

B2. Bond, J. W., Watson, K. M., and Welch, J. A., Atomic Theory of Gas
      Dynamics, Addison-Wesley, Reading, MA, 1965, p. 100.

B3. Bond, J. W., Watson, K. M., and Welch, J. A., Atomic Theory of Gas
      Dynamics, Addison-Wesley, Reading, MA, 1965, p. 86.

B4. Zel'dovich, Y. B., and Raizer, Y. P., Physics of Shock Waves and
      High Temperature Hydrodynamic Phenomena, Volume 1, Academic

B5. Svehla, R. A., "Thermodynamic and Transport Properties for the
      Hydrogen-Oxygen System," NASA SP-3011, 1964.

C1. Vincenti, W. G. and Kruger, C. H., Introduction to Physical Gas
      Dynamics, John Wiley and Sons, New York, 1965, p. 298.

APPENDIX A

CONICAL FLOWFIELD AVERAGING

APPENDIX A NOMENCLATURE

A = area, m^2

C_p = constant pressure specific heat, J/Kg°K

h = enthalpy, J/Kg

$\dot{m}$ = mass flow rate, Kg/s

$\hat{n}$ = normal to a control surface

P = static pressure, Pa

P_T = stagnation pressure, Pa

R = radial distance, m

r = radial direction subscript

T = static temperature, °K

T_T = stagnation temperature, °K

V = velocity, m/s

δ = conical diffuser half-angle, radians

γ = ratio of specific heats

ρ = density, Kg/m^3

θ_s = conical shock half-angle, radians

A bar over any variable indicates that this variable represents an average value, a numerical subscript denotes a position shown in Figure A1, and a subscript of r or θ indicates a direction as specified in Figure A2.

APPENDIX A

CONICAL FLOWFIELD AVERAGING

In this analysis it is assumed that the working fluid behaves as a perfect gas, and that the flowfield is axis-symmetric and quasi-steady. Assuming that the working fluid behaves as a perfect gas should not introduce too much error because for shallow cone angles the flowfield conditions should not change significantly across a conical shock even for high incoming Mach numbers. The quasi-steady assumption is justified in Appendix D where it is shown that fluid particle residence times are small compared to the times required for flowfield changes to be significant. The geometric constraints should not let the ramjet projectile deviate significantly from axis-symmetric conditions, so assuming axis-symmetric flowfields exist should not introduce significant errors.

Consider a conical diffuser of the type shown in Fig. A1 to be operating at a zero angle of attack within a launch tube. Assume that the projectile is traveling at a high enough velocity so that conical shock attachment is assured. The conical shock formed will intersect the tube wall as shown in Figure A1. For a given conical half-angle (δ) the flow from 1 to 2 can be calculated given conditions at 1 using the Taylor-Maccol method.[A1] Indeed, the conditions anywhere within the axis-symmetric flowfield can be calculated using this method. The problem is to describe the flow between 1 and 4 for given conditions at 1 and a specified diffuser geometry. In reality a pattern of reflected oblique shock waves would exist downstream of the initial conical shock depending on the annular diffuser throat area and the
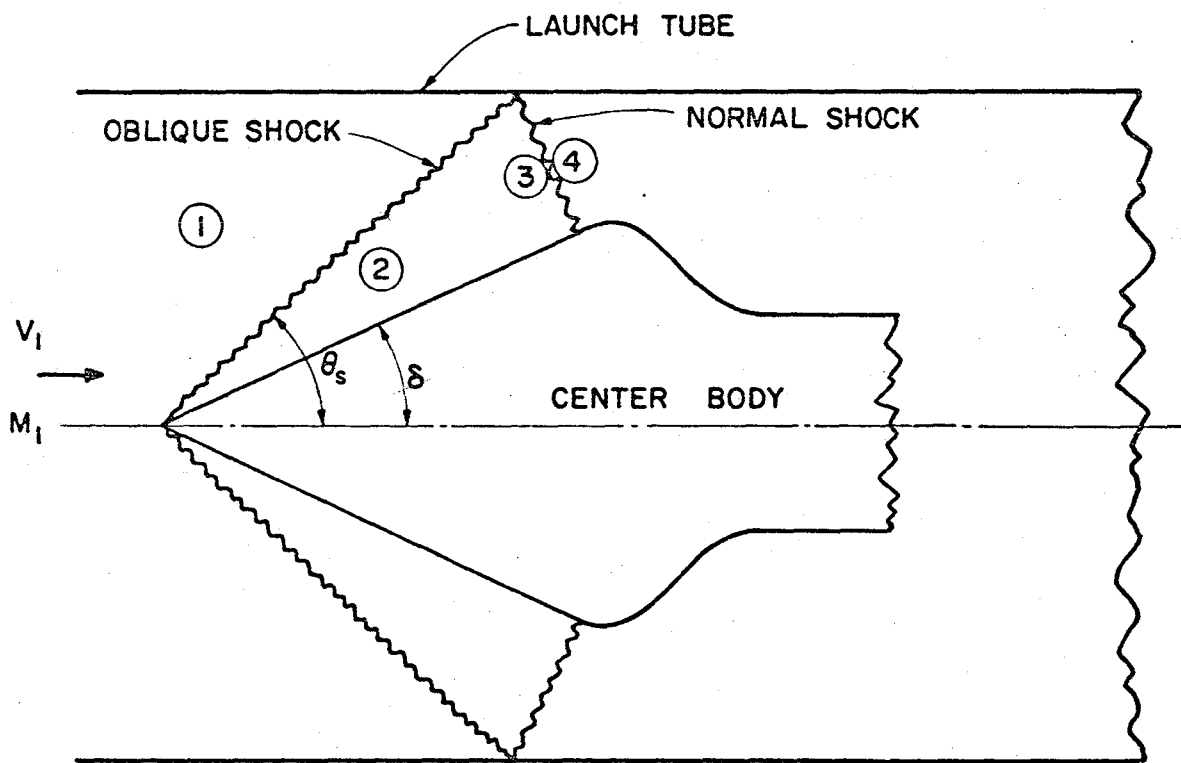
Fig. A1 Electrothermal Ramjet Diffuser

pressure at 4. If it happens that the flow is restricted at the diffuser throat or downstream of 4 then a bow shock could exist ahead of the diffuser. If the downstream conditions are selected as they are for designs considered here so that the flow is not restricted and that the back pressure conditions are correct then a reflected shock pattern terminated by a normal shock will exist. The location of the terminating normal shock can be dictated by varying the diffuser throat area and the pressure at 4.

For hypersonic flows, because of separation and boundary layer-shock wave interaction effects, diffusers perform close to what is predicted for normal shock diffusers.[A2] Thus in this analysis the following assumptions are used:

1) The separation and boundary layer-shock interaction behavior does not become important until the reflected shock pattern begins downstream of the intersection of the tube wall with the initial conical shock. Neglecting separation and boundary layer effects in this initial conical flowfield region should not produce large errors because the scale of the diffuser is expected to be small. Neglecting these effects also allows the Taylor-Maccol method of analyzing conical flowfields to be utilized.

2) The flow downstream of the initial conical flowfield is rapidly mixed and can be modeled by a one-dimensional flow which satisfies the conservation laws. It is noted that the conservation laws are insufficient to completely specify the one-dimensional flow; an additional assumption which will be described shortly is also needed.

3) A normal shock terminates the one-dimensional supersonic flowfield.

When these assumptions are applied the flow processes in the diffuser can be modelled in the following way suggested by Fig. A1. The free stream flow passes from state 1 through the conical shock into the conical flowfield of region 2. The properties of this flowfield, which vary from point to point and must be calculated using a numerical procedure, are averaged over the surface immediately upstream of the normal shock to obtain the properties at 3. These averaged properties serve as input to the one-dimensional normal shock relations and yield the properties of the fluid immediately downstream of the normal shock at state 4.

The additional statement needed to connect the conical and one-dimensional flowfields will now be considered. The choice used here is made through the definition of a mass flow rate averaged velocity for the conical flowfield and equating this to a characteristic one-dimensional velocity $\bar{V}_3$. In Fig. A1 let states 2 and 3 represent the conical and one-dimensional flowfield states respectively. The mass flow rate average velocity at 3 is defined by

$$\bar{V}_3 = \frac{\int_{c.s.} |\vec{V}| \, \rho(\vec{V} \cdot \hat{n}) \, dA}{\int_{c.s.} \rho(\vec{V} \cdot \hat{n}) \, dA}$$

where the subscript c.s. refers to any arbitrary control surface which the complete conical flowfield passes through. The integration is simplified if a spherical coordinate system is placed at the vertex of the physical cone and the control surface is taken to be a spherical cap

as is shown in Figure A2.

For this choice

$$\vec{V} \cdot \hat{n} = V_r = \text{velocity in the radial direction}$$

$$|\vec{V}| = (V_r^2 + V_\theta^2)^{\frac{1}{2}}$$

$$\rho = \rho(\theta) \quad \text{[for conical flow]}$$

$$dA = 2\pi R^2 \sin\theta \, d\theta \quad .$$

Thus it follows that

$$\overline{V}_3 = \frac{\int_\delta^{\theta_s} \rho \, (V_r^2 + V_\theta^2)^{\frac{1}{2}} V_r \, 2\pi R \, \sin\theta \, d\theta}{\int_\delta^{\theta_s} \rho \, V_r \, 2\pi R^2 \, \sin\theta \, d\theta} \quad .$$

In this expression the factor $2\pi R^2$ appears in both the numerator and denominator and thus will cancel. This implies that the one-dimensional properties of a conical flowfield are independent of the scale of the flow conditions. It follows then that the value for the average velocity immediately upstream of the normal shock is calculated from

$$\overline{V}_3 = \frac{\int_\delta^{\theta_s} \rho \, V_r (V_r^2 + V_\theta^2)^{\frac{1}{2}} \sin\theta \, d\theta}{\int_\delta^{\theta_s} \rho \, V_r \, \sin\theta \, d\theta} \quad .$$

Mass continuity, which must also be satisfied in the conical flowfield, requires that

$$\overline{\rho}_3 \, \overline{V}_3 \, A_3 = \int_\delta^{\theta_s} 2\pi R^2 \, \rho \, V_r \, \sin\theta \, d\theta = \dot{m}_3$$
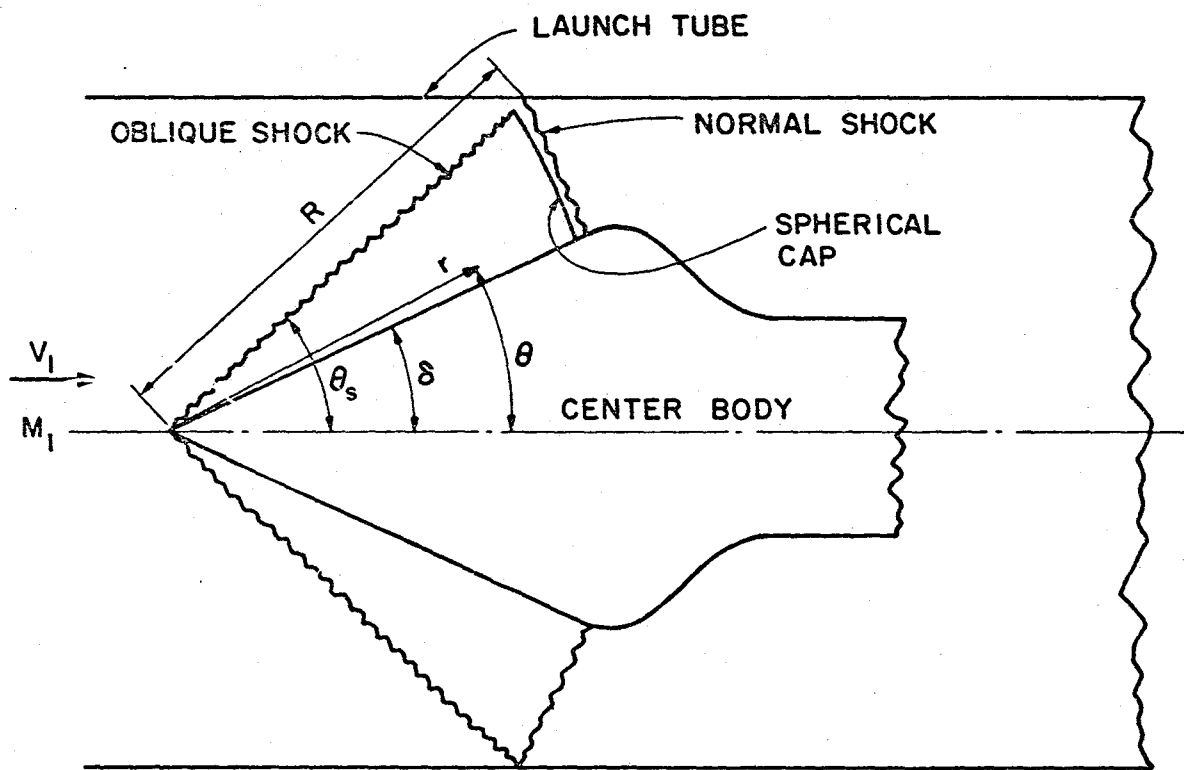
Fig. A2   Conical Flow Coordinate System

where

$$A_3 = 2\pi R^2 \int_\delta^{\theta_S} \text{Sin}\theta \, d\theta = -2\pi R^2 (\text{Cos}\theta_S - \text{Cos}\delta).$$

Combining these expressions one obtains an expression for the mean density immediately upstream of the normal shock.

$$\bar{\rho}_3 = \frac{\int_\delta^{\theta_S} \rho \, V_r \, \text{Sin}\theta \, d\theta}{\bar{V}_3 (\text{Cos}\delta - \text{Cos}\theta_S)}$$

The first law of thermodynamics must also be satisfied.

$$h_{T_3} = h_{T_1} = C_p \bar{T}_3 \left[1 + \frac{\gamma-1}{2} M_3^2\right]$$

Solving for the mean temperature upstream of the normal shock yields

$$\bar{T}_3 = \frac{h_{T_1}}{C_p} - \frac{\gamma-1}{\gamma} \frac{\bar{V}_3^2}{2R} \quad .$$

The ideal gas equation is assumed to be valid.

$$\bar{P}_3 = \bar{\rho}_3 R \bar{T}_3$$

The average stagnation pressure is defined by

$$\bar{P}_{T_3} = \bar{P}_3 \left(\frac{T_{T_3}}{\bar{T}_3}\right)^{\frac{\gamma}{\gamma-1}} \quad .$$

These average values for the flowfield variables are used as input for the normal shock relations.

The only criterion applied to determine the annular diffuser throat area is that this area be large enough to swallow the flow downstream of the normal shock.

The Taylor-Maccol method of analyzing conical flowfields, which was utilized in the analyses conducted in this thesis, is not presented. For a complete description of this procedure see reference A1.

APPENDIX B

EQUILIBRIUM HYDROGEN PROPERTIES

APPENDIX B NOMENCLATURE

A = Helmholtz function, J

D_o = diatomic hydrogen dissociation energy, 7.171×10^{-19} J

ΔE_{ion_i} = lowering of the ionization potential for specie i, J

e = electron charge, 1.6021×10^{-19} Coulomb

g = degeneracy

h = Planck's constant, 6.62517×10^{-34} J-sec

h = enthalpy per unit mass, J/Kg

$\bar{h}$ = enthalpy per unit mole, J/Kmole

K = Boltzmann's constant, 1.3804×10^{-23} J/°K

M_i = molecular weight of specie i, Kg/Kmole

m_i = mass of specie i

N_i = number of particles of specie i

n_{ion} = number density of ions, m^{-3}

P = pressure, Pa

Q_i = charge of specie i

R = universal gas constant, 8.314 J/mole°K

S = entropy, J/°K

s = entropy per unit mass, J/Kg°K

$\bar{s}$ = entropy per unit mole, J/mole°K

T = temperature, °K

U = internal energy, J

u = internal energy per unit mass, J/Kg

$\bar{u}$ = internal energy per unit mole, J/mole

Ψ = volume, m^3

$\bar{v}_i$ = molar specific volume of specie i, m^3/mole

Y_i = mole fraction of specie i

Z_i = partition function for specie i

ε_i = electronic energy of the ith level for a given specie, J

ε_i = electron affinity for the ith specie, J

ε_i = ionization energy for the ith specie, J

APPENDIX B

EQUILIBRIUM HYDROGEN PROPERTIES

In analyzing ramjet operation it is necessary to calculate the equilibrium composition and thermodynamic properties for hydrogen. This is done by the methods presented in this Appendix. The species considered in this analysis are

$$H_2, H_2^+, H, H^+, H^-, e^- \ .$$
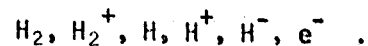
When a mixture of these species is at equilibrium the Helmholtz function

$$A = U - TS$$

is at a minimum. In this analysis it is assumed that the Helmholtz function can be expressed in the form

$$A = A_{pg} + A_c$$

where A_{pg} is the perfect gas Helmholtz function, which is valid for noninteracting particles, and A_c is the coulombic interaction Helmholtz function which comes into play for the case where the mixture is ionized. The coulombic term can be considered as a correction to the perfect gas form. The perfect gas term can be expressed in the form

$$A_{pg} = - KT \ [\sum_i N_i (\ln(\frac{Z_i}{N_i}) + 1)]$$

where N_i is the number of particles of the ith specie and (Z_i/N_i) is the perfect gas partition function for the ith specie. The coulombic term

can be expressed in the form

$$A_c = - \frac{2}{3} e^3 \left(\frac{\pi}{KT\Psi}\right)^{\frac{1}{2}} (\Sigma N_i Q_i^2)^{3/2}$$

where Q_i is the charge of the ith specie and e is the charge on an electron. At equilibrium

$$dA = dA_{pg} + dA_c = 0 \quad .$$

The differentiation is taken to occur at a constant temperature and volume. Variations in the Helmholtz function due to changes in the composition are considered. The forms for the differentials are

$$dA_{pg} = - KT \Sigma \ell n \left(Z_i/N_i\right) dN_i$$

and

$$dA_c = -e^3 \left(\frac{\pi}{KT\Psi}\right)^{\frac{1}{2}} \left[\Sigma N_i Q_i^2\right]^{\frac{1}{2}} \left[\Sigma Q_i^2 dN_i\right] \quad .$$

Combining these expressions yields

$$\Sigma \ell n \frac{Z_i}{N_i} dN_i + \frac{e^3}{(KT)^{3/2}} \left(\frac{\pi}{\Psi}\right)^{\frac{1}{2}} \left[\Sigma N_i Q_i^2\right]^{\frac{1}{2}} \left[\Sigma Q_i^2 dN_i\right] = 0 \quad .$$

This expression can be put into a slightly different form

$$\Sigma \ell n \frac{Z_i}{N_i} dN_i + \Sigma \left\{ \frac{e^3}{(KT)^{3/2}} \left(\frac{\pi}{\Psi}\right)^{\frac{1}{2}} \left[\Sigma N_i Q_i^2\right]^{\frac{1}{2}} Q_i^2 dN_i \right\} = 0 \quad .$$

Factoring out dN_i yields

$$\Sigma \left\{ \ell n \frac{Z_i}{N_i} + \frac{e^3}{(KT)^{3/2}} \left(\frac{\pi}{\Psi}\right)^{\frac{1}{2}} \left[\Sigma N_i Q_i^2\right]^{\frac{1}{2}} Q_i^2 \right\} dN_i = 0$$

or

$$\Sigma J_i dN_i = 0$$

where

$$J_i \equiv \ln \frac{Z_i}{N_i} + \frac{e^3}{(KT)^{3/2}} \left(\frac{\pi}{V}\right)^{\frac{1}{2}} \left[\Sigma N_i Q_i^2\right]^{\frac{1}{2}} Q_i^2 \ .$$

The chemical reactions considered are

$$\rho_a \qquad H_2 \overset{\leftarrow}{\to} 2H \qquad\qquad a)$$

$$\rho_b \qquad H_2 \overset{\leftarrow}{\to} H_2^+ + e^- \qquad b)$$

$$\rho_c \qquad H \overset{\leftarrow}{\to} H^+ + e^- \qquad c)$$

$$\rho_d \qquad H^- \overset{\leftarrow}{\to} H + e^- \ . \qquad d)$$
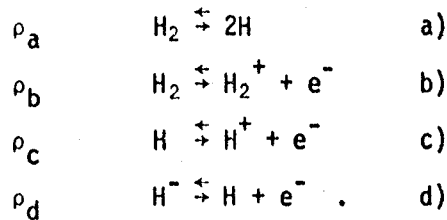
where the degree of reaction for each chemical reaction is defined as being the variable ρ. If each reaction is assumed to proceed slightly from left to right then the change in each component is given by

$$dN_{H_2} = -d\rho_a - d\rho_b$$

$$dN_{H_2}^+ = d\rho_b$$

$$dN_H = 2 d\rho_a - d\rho_c + d\rho_d$$

$$dN_H^+ = d\rho_c$$

$$dN_H^- = -d\rho_d$$

$$dN_e^- = d\rho_b + d\rho_c + d\rho_d \ .$$

By combining these expressions with the expression

$$\Sigma J_i \, dN_i = 0$$

the following equation can be obtained

$$(-J_{H_2} + 2J_H) \, d\rho_a + (-J_{H_2} + J_{H_2}^+ + J_{e^-}) \, d\rho_b +$$

$$(-J_H + J_H^+ + J_{e^-}) \, d\rho_c + (-J_H^- + J_H + J_{e^-}) \, d\rho_d = 0 \ .$$

Since the chemical reactions and hence the $d\rho$ values are assumed to be

independent, each quantity in brackets must be equal to zero at equilibrium. This equation is used to help determine the chemical equilibrium composition.

Consider the reaction

$$H_2 \leftrightarrows 2H \quad .$$
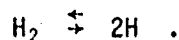
For this reaction the relation

$$-J_{H_2} + 2J_H = 0$$

is used. In more complete form this equation becomes

$$\ln \frac{Z_{H_2}}{N_{H_2}} + \frac{e^3}{(KT)^{3/2}} \left(\frac{\pi}{V}\right)^{\frac{1}{2}} \left[\Sigma N_i Q_i^2 \right]^{\frac{1}{2}} Q_{H_2}^2$$

$$= 2 \ln \frac{Z_H}{N_H} + \frac{2e^3}{(KT)^{3/2}} \left(\frac{\pi}{V}\right)^{\frac{1}{2}} \left[\Sigma N_i Q_i \right]^{\frac{1}{2}} Q_H^2$$

but

$$Q_{H_2} = Q_H = 0$$

so this equation degenerates to

$$\frac{Z_H^2}{Z_{H_2}} = \frac{N_H^2}{N_{H_2}}$$

which is the correct form for a conventional perfect gas analysis. Multiplying each side of the equation by

$$\frac{\Sigma N_i}{(\Sigma N_i)^2} = \frac{N}{N^2}$$

allows this equation to be put into the form

$$\frac{Y_H^2}{Y_{H_2}} = \frac{(Z/N)_H^2}{(Z/N)_{H_2}}$$

where N is total number of particles.

For the reaction

$$H_2 \leftrightarrows H_2^+ + e^-$$
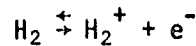
the relation

$$-J_{H_2} + J_{H_2^+} + J_{e^-} = 0$$

is valid. In its more complete form this equation becomes

$$\ell n \; \frac{Z_{H_2}}{N_{H_2}} + \frac{e^3}{(KT)^{3/2}} \left(\frac{\pi}{V}\right)^{\frac{1}{2}} \left[\Sigma N_i Q_i^2\right]^{\frac{1}{2}} Q_{H_2}^2 =$$

$$\ell n \; \frac{Z_{H_2^+}}{N_{H_2^+}} + \ell n \; \frac{Z_{e^-}}{N_{e^-}} + \frac{e^3}{(KT)^{3/2}} \left(\frac{\pi}{V}\right)^{\frac{1}{2}} \left[Q_{H_2^+}^2 + Q_{e^-}^2\right] \left[\Sigma N_i Q_i^2\right]^{\frac{1}{2}}$$

where

$$Q_{H_2} = 0$$

$$Q_{H_2^+} = +1$$

$$Q_e = -1 \; .$$

After rearrangement this equation degenerates to

$$\ell n \; \left\{\left(\frac{Z_{H_2}}{Z_{H_2} \; Z_{e^-}}\right)\left(\frac{N_{H_2^+} \; N_{e^-}}{N_{H_2}}\right)\right\} = 2e^3 \; \frac{\pi^{\frac{1}{2}}}{(KT)^{3/2}} \; n_{ion}^{\frac{1}{2}}$$

where the parameter n_{ion} is defined by

$$n_{ion} = \frac{\Sigma N_i Q_i^2}{V}$$

and represents the ion number density.   Rearranging and multiplying
through by N/N^2 yields

$$\frac{Y_{H_2^+} Y_{e^-}}{Y_{H_2}} = \frac{(Z/N)_{H_2^+} (Z/N)_{e^-}}{(Z/N)_{H_2}} \quad \exp\left\{\left(\frac{2e^3 \, \pi^{\frac{1}{2}} n_{ion}^{\frac{1}{2}}}{(KT)^{\frac{1}{2}}}\right)\left(\frac{1}{KT}\right)\right\} \quad .$$

For the case where n_{ion} is a small number, the exponential term on the
right hand side of the above equation will be close to one, which cor-
responds to the form obtained when only a perfect gas analysis is done
(i.e. the Saha Equation). When the number density of ions is signifi-
cant, however, a coulombic field will be present, and this field will
affect the ionization of the different particles. The net effect of
this coulombic field is to decrease the amount of energy needed to re-
move an electron from the influence of a given nucleus (the ionization
energy is decreased). Consequently, the exponential term in the
preceding equation can be thought of as representing an expression for
the lowering of the ionization potential. The lowering of the ioniza-
tion potential can therefore be expressed as

$$\Delta E_{ion \atop H_2} = 2e^3 \left(\frac{\pi \, n_{ion}}{KT}\right)^{\frac{1}{2}}$$

and the expression for the mole fraction ratio becomes

$$\frac{Y_{H_2^+} Y_{e^-}}{Y_{H_2}} = \frac{(Z/N)_{H_2}(Z/N)_{e^-}}{(Z/N)_{H_2}} \quad \exp\left(\frac{\Delta E_{ion \atop H_2}}{KT}\right) .$$

For the chemical reaction

$$H \rightleftharpoons H^+ + e^-$$
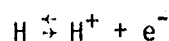
the same form is obtained for the expression for the mole fraction
ratio namely

$$\frac{Y_{H^+}\, Y_{e^-}}{Y_H} = \frac{(Z/N)_{H^+}\, (Z/N)_{e^-}}{(Z/N)_H} \,\exp\left(\frac{\Delta E_{ion}}{KT}\right)_H$$

where

$$\Delta E_{ion_H} = 2e^3 \left(\frac{\pi\, n_{ion}}{KT}\right)^{\frac{1}{2}} = \Delta E_{ion_{H_2}} \qquad .$$

An interesting result is obtained when the reaction

$$H^- \; \overset{\leftarrow}{\rightarrow} \; H + e^-$$
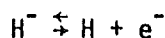
is considered. For this reaction the relation

$$J_{H^-} \;=\; J_H + J_{e^-}$$

is valid. When this equation is expanded it assumes the following
form

$$\ell n\,\frac{Z_{H^-}}{N_{H^-}} + \frac{e^3}{(KT)^{3/2}}\,\left(\frac{\pi}{\Psi}\right)^{\frac{1}{2}}\,\left[\Sigma N_i Q_i^2\right]^{\frac{1}{2}}\,Q_{H_2^-}^2 =$$

$$\ell n\,\frac{Z_H}{N_H} + \ell n\,\frac{Z_{e^-}}{N_{e^-}} + \frac{e^3}{(KT)^{3/2}}\,\left(\frac{\pi}{\Psi}\right)^{\frac{1}{2}}\,\left[\Sigma N_i Q_i^2\right]^{\frac{1}{2}}\,Q_{e^-}^2$$

where

$$Q_{e^-}^2 = Q_{H^-}^2 = 1 \qquad .$$

The coulombic interaction terms will cancel so this equation assumes
the form

$$\frac{Z_H\, Z_{e^-}}{Z_{H^-}} = \frac{N_H\, N_{e^-}}{N_{H^-}}$$

which predicts that, for a negative ion, there is no lowering of the ionization potential. However, if the negative ion was doubly charged and only one electron was removed, then a change in the ionization potential would be predicted. Multiplying the previous equation by N/N^2 yields

$$\frac{Y_H Y_{e^-}}{Y_{H^-}} = \frac{(Z/N)_H \ (Z/N)_{e^-}}{(Z/N)_{H^-}} \quad .$$

At this point in the analysis, four equations describing the relationships of the mole fraction species have been derived. In summary, these equations are

$$\frac{(Y_H)^2}{Y_{H_2}} = \frac{(Z/N)_H^2}{(Z/N)_{H_2}}$$

$$\frac{Y_{H_2^+} \ Y_{e^-}}{Y_{H_2}} = \frac{(Z/N)_{H_2^+} \ (Z/N)_{e^-}}{(Z/N)_{H_2}} \ \exp\left[\frac{\Delta E_{ion_{H_2}}}{KT}\right]$$

$$\frac{Y_{H^+} \ Y_{e^-}}{Y_H} = \frac{(Z/N)_{H^+} \ (Z/N)_{e^-}}{(Z/N)_H} \ \exp\left[\frac{\Delta E_{ion_H}}{KT}\right]$$

$$\frac{Y_H \ Y_{e^-}}{Y_{H^-}} = \frac{(Z/N)_H \ (Z/N)_{e^-}}{(Z/N)_{H^-}} \quad .$$

However, because there are six species considered, two more equations must be obtained in order to ensure a unique solution. One of these two equations can be derived by assuming that charge is conserved

$$Y_{H^+} + Y_{H_2^+} - Y_{e^-} - Y_{H^-} = 0 \quad .$$

The second equation comes from summing up the mole fractions

$$Y_{H_2} + Y_{H_2^+} + Y_H + Y_{H^+} + Y_{H^-} + Y_{e^-} = \frac{\Sigma\, n_i}{n} = 1 \; .$$

The variable $(Z/N)_i$ is the partition function for the ith specie evaluated at the total system pressure and temperature. In order to evaluate the partition function it is necessary to select an energy datum, and the datum selected for this analysis is the ground electronic state of the H_2 molecule at $0°K$. The partition function of each specie is computed relative to this state.

The partition function for any specie i can be expressed in the form

$$(Z/N)_i = \left(\frac{Z_t}{N}\right)_i \left(Z_{internal}\right)_i$$

where the translational contribution is given by

$$(Z_t/N)_i = \left(\frac{2\pi\, m_i}{h^2}\right)^{3/2} \frac{(KT)^{5/2}}{P} \; .$$

The form of the internal contribution varies depending on whether the specie under consideration is diatomic or monatomic. A diatomic specie will have rotational and vibrational contributions, and the diatomic species and some of the monatomic species will have electronic contributions. The possibility of having a chemical energy contribution to the internal partition function also exists for some of the monatomic and diatomic species, notably H_2^+, H, H^+, H^-, and e^-, depending on where the ground state energy of the given specie relative to the datum selected above lies.

Consider the monatomic specie of neutral hydrogen (H). The internal partition function for H is given by

$$Z_{internal \atop H} = Z_{chem \atop H} \, Z_{elec \atop H}$$

where

$$Z_{chem \atop H} = \exp\left(-\frac{D_o}{2KT}\right)$$

and

$$Z_{elec \atop H} = \sum_{e_j} g_{e_j} \exp\left(-\frac{\epsilon_{e_j}}{KT}\right) \,.$$

This expression assumes that each H atom receives 1/2 of the chemical energy required to dissociate a ground state H_2 molecule. The degeneracy (g_{e_j}) in the electronic contribution relation is given by

$$g_{e_j} = 2j^2 \qquad j = 1, 2, 3, \ldots .$$

and the energy (ϵ_{e_j}) is given by

$$\epsilon_j = \left(\frac{2\pi^2 C^2 L^2 e^4 m}{h^2}\right) \frac{j^2-1}{j^2} \qquad j = 1, 2, 3, \ldots .$$

In this equation for the energy state, L is the charge of the nucleus (1 for H), e is the electron charge, m is the electron mass, h is Planck's constant and C is a proportionality constant. Inserting these relations into the expression for the electronic partition function for the hydrogen (H) atom yields

$$Z_{elec \atop H} = \sum_{j=1}^{J} 2j^2 \exp\left[\frac{2\pi^2 C^2 L^2 e^4 m}{h^2 KT} \, \frac{1-j^2}{j^2}\right] \,.$$

Examination of this equation brings to light the fact that the series
will diverge unless a cutoff (J) for the summation is specified. A
method of calculating this cutoff will be given later in this Appendix.

The other monatomic species are H^+, e^- and H^-. For the H^+ particle
the value for the internal partition function is 1, and the chemical
partition function is given by

$$Z_{chem \atop H^+} = \exp\left[\frac{-(D_0/2 + \varepsilon_{i_H})}{KT}\right] \quad .$$

In this expression ε_{i_H} is the ionization energy of a hydrogen atom.
The H^+ particle is assumed to carry all of the ionization energy. For
the electron (e^-) the internal partition function is

$$Z_{int \atop e^-} = 2$$

because of the spin contribution to the degeneracy. The electron is
assumed to carry no chemical energy so the chemical contribution to the
partition function is

$$Z_{chem \atop e^-} = 1 \quad .$$

The H^- ion has an electron affinity value (ε_{affin}) that must be taken
into account when calculating the chemical partition function. The
chemical partition function is given by

$$Z_{chem \atop H^-} = \exp\left[\frac{-(D_0/2 + \varepsilon_{affin})}{KT}\right] \quad .$$

Only the ground electronic state is considered for the H^- ion and

the internal partition function (electronic) is

$$Z_{int_{H^-}} = 1.$$

Higher electronic states are neglected because the existence of electronically excited negative ions is rare.[B1] The binding energy for a negative ion is generally small and it is not too difficult to remove an electron from a negatively charged particle. Also, because the binding energy is small, it seems to make sense to neglect electronic states above the ground state because the higher electronic states effectively reduce the amount of energy required to remove an electron. The binding energy for the extra electron on a negative ion is not large because the inner electron(s) repel the extra electron with a charge that is equal to the charge of the nucleus, effectively shielding the extra electron from the nucleus.

For the diatomic species (H_2, H_2^+) there are rotational and vibrational contributions to the internal partition functions that must be taken into account. In this analysis coupling between the rotational and vibrational energy storage modes is allowed, and an expression characterizing the rotational and vibrational modes for separate electronic levels is presented later in this Appendix. The complete internal partition function for the H_2 molecule (and H_2^+) is expressed by

$$Z_{int} = \sum_{\substack{all \\ e_j}} Z_{rv_{e_j}} Z_{e_j}$$

where the summation must be terminated at a finite electronic energy level. The internal partition function is more completely expressed in

the form

$$Z_{int} = \sum_{\substack{all \\ e_j}} g_{e_j} \exp\left(\frac{-\epsilon_{e_j}}{KT}\right) \frac{1}{\sigma y} \left(\frac{1}{1-e^{-t}}\right)$$

$$\left\{ 1 + \frac{y}{3} + \frac{2\gamma}{y} + \frac{\delta}{e^t - 1} + \frac{2x^* t}{(e^t - 1)^2} \right\} \quad .$$

In this expression $\sigma = 2$ because a diatomic molecule is symmetric. The following parameters are evaluated from the rotational and vibrational constants for the given electronic levels (the rotational and vibrational constants can be found in compilations such as the one in Reference B2).

$$t = \frac{hc}{KT} (W_\epsilon - X_\epsilon W_\epsilon)$$

$$x^* = \frac{X_\epsilon W_\epsilon}{W_\epsilon - X_\epsilon W_\epsilon}$$

$$y = \frac{hc}{KT} (B_\epsilon - 1/2 \, \alpha_\epsilon)$$

$$\delta = \frac{\alpha}{B_\epsilon - 1/2 \, \alpha_\epsilon}$$

$$\gamma = \frac{D_\epsilon}{B_\epsilon - 1/2 \, \alpha_\epsilon} \quad .$$

The parameters W_ϵ, $X_\epsilon W_\epsilon$, B_ϵ, and α_ϵ are the rotational and vibrational constants and D_ϵ is computed using

$$D_\epsilon = \frac{4 \, B_\epsilon^3}{W_\epsilon^2} \quad .$$

The H_2^+ molecule has a chemical (ionization) energy that must be taken into account, and the chemical partition function for H_2^+ is given by

$$Z_{\substack{chem \\ H_2^+}} = \exp\left(\frac{-\epsilon_{i_{H_2}}}{KT}\right) .$$

It should be explained here that the ionization energies used in evaluating the partition functions are values published in a reference such as Reference B3. It is assumed that these values were obtained for rarified, very weakly ionized gases where coulombic interactions are unimportant. The calculation of the ionization energy for a given specie takes the published value as a baseline, and this value is then changed in the manner detailed earlier where the changes in ionization energies are defined for the different species.

In the evaluation of the various partition functions it is necessary to specify cutoff values whenever electronic levels other than the ground level are considered. In essence, the problem is establishing a criterion for when an electron can no longer be considered to be bound to the nucleus of an atom or to the nuclei of a molecule. The criterion selected for this analysis is to not allow any electronic energies which exceed the ionization energy (taking into account the lowering of the ionization energy discussed earlier).

Solving for the equilibrium composition is an iterative process because the equations are nonlinear and the lowering of the ionization potential must be determined implicitly. The method used in this analysis is to assume initially that no ions are present and to apply the model just presented and compute the ion density. A new ion density based on the computed value is then used as input and this process

continues until the difference between the assumed and computed ion density is sufficiently small. The value required for the number density of the ions (n_{ion}) is computed from

$$n_{ion} = \frac{N_{ion}}{V} = \frac{N}{V} \frac{N_{ion}}{N} = \frac{P}{KT} \left(Y_{e^-} + Y_{H^-} + Y_{H^+} + Y_{H_2^+} \right) \quad .$$

Once the equilibrium composition has been found, the thermodynamic properties of the mixture must also be evaluated. It is noted that the coulombic corrections previously referred to in this Appendix will affect the composition and the thermodynamic properties of the species because the ionization energies and the allowed electronic excitation levels are changed by allowing coulombic corrections to appear. Also, the coulomb field itself will possess definite thermodynamic properties and these properties will contribute to the thermodynamic state of the complete hydrogen mixture. For example, the ions will be slightly attracted to each other so that the actual system pressure will be slightly less than is predicted by the ideal gas equation. However, in the spirit of Reference B4, it is assumed in this analysis that the contribution of the coulombic field to the total system thermodynamic state of a hydrogen mixture is small and can therefore be neglected without introducing significant error.

The entropy ($\bar{s}$), enthalpy ($\bar{h}$) and internal energy ($\bar{u}$) of a mixture can be expressed on a molar basis by the following relations

$$\bar{s} = \sum Y_i \, \bar{s}_i$$
$$\bar{h} = \sum Y_i \, \bar{h}_i$$
$$\bar{u} = \sum Y_i \, \bar{u}_i \quad .$$

Dividing each equation through by the average molecular weight which is defined by

$$M_{ave} = \sum Y_i M_i$$

allows these properties to be expressed on a per unit mass basis

$$s = \frac{\sum Y_i \bar{s}_i}{\sum Y_i M_i}$$

$$h = \frac{\sum Y_i \bar{h}_i}{\sum Y_i M_i}$$

$$u = \frac{\sum Y_i \bar{u}_i}{\sum Y_i M_i} \quad .$$

The internal energy on a molar basis of a specie i ($\bar{u}_i$) can be expressed in the form

$$\bar{u}_i = RT^2 \left(\frac{\partial \ln Z_i}{\partial T} \right)_{V_i} \quad .$$

Since the enthalpy ($\bar{h}_i$) is defined by

$$\bar{h}_i = \bar{u}_i + P_i \bar{v}_i$$

where $\bar{v}_i$ is the molar specific volume, and the ideal gas equation

$$P_i \bar{v}_i = RT$$

is assumed to be valid, the enthalpy per mole can be expressed in the form

$$\bar{h}_i = RT^2 \left(\frac{\partial \ln Z_i}{\partial T} \right)_{V_i} + RT \quad .$$

The entropy per unit mole is expressed by

$$\bar{s}_i = R \left\{ \ln \frac{Z_i}{N_i} + 1 \right\} + \frac{\bar{u}_i}{T} \quad .$$

The variable R is the universal gas constant.

In order that the thermodynamic properties can be calculated the partial derivative appearing in the thermodynamic relations is expressed in the form

$$\left(\frac{\partial (\ln Z_i)}{\partial T} \right)_{\Psi_i} = \frac{1}{Z_i} \left(\frac{\partial Z_i}{\partial T} \right)_{\Psi_i} \quad .$$

It is possible to separate the translational partition function out of this expression. The partial derivative of the translational partition function for any specie is given by

$$\frac{1}{Z_{trans}} \left(\frac{\partial Z_{trans}}{\partial T} \right)_{\Psi_i} = \frac{3}{2} \frac{1}{T} \quad .$$

Consequently, the translational contributions to the internal energy and enthalpy are given by

$$\bar{u}_{i_{trans}} = 3/2 \ RT$$

$$\bar{h}_{i_{trans}} = 5/2 \ RT \quad .$$

When the chemical energy is considered, the internal energy and enthalpy are given by

$$\bar{u}_{i_{chem}} = \bar{h}_{i_{chem}} = N_0 \ (D_0/2 + \varepsilon_i)$$

where D_0 is the dissociation energy and ε_i is the ionization energy.

The electronic contribution to the thermodynamic preoperties must be accounted for in the monatomic hydrogen (H) atom. The form for the partial derivative is

$$\frac{\partial(\ln Z_{elec_H})}{\partial T} = \frac{F}{KT^2} \frac{\sum\limits_{j=1}^{J} (j^2-1) \exp\left(\frac{-F}{KT} \frac{j^2-1}{j^2}\right)}{\sum\limits_{j=1}^{J} j^2 \exp\left(\frac{-F}{KT} \frac{j^2-1}{j^2}\right)} \quad .$$

The value obtained in this summation is utilized to calculate the enthalpy ($\bar{h}$) and the internal energy ($\bar{u}$) for the hydrogen atom. The constant F is given by

$$F = \frac{2\pi^2 C^2 L^2 e^4 m}{h^2} \quad .$$

For the diatomic species the internal contributions to the partition function are given by

$$Z_{int} = \sum\limits_{e_j} Z_{rv_{ej}} Z_{e_j} \quad .$$

Consequently the partial derivative is evaluated in the form

$$\left(\frac{\partial(\ln Z_{int})}{\partial T}\right)_\Psi = \frac{\sum\limits_{e_j} Z_{rv_{ej}} \left(\frac{\partial Z_{e_j}}{\partial T}\right)_\Psi + Z_{e_j} \left(\frac{\partial Z_{rv_{ej}}}{\partial T}\right)_\Psi}{\sum\limits_{e_j} Z_{rv_{ej}} Z_{e_j}} \quad .$$

For a given electronic energy e_j the partial derivative of the electronic contribution function is given by

$$\left(\frac{\partial Z_{e_j}}{\partial T}\right)_V = g_j \frac{\epsilon_j}{KT^2} \exp\left(-\frac{\epsilon_j}{KT}\right) \ .$$

The expression for the partial derivative of the rotational-vibrational term is given below

$$\frac{\partial (Z_{rv})_{e_j}}{\partial T} = AB + CD$$

where the parameters A, B, C, and D are evaluated using

$$A = \frac{1}{\sigma y} \ \frac{1}{1-e^{-t}}$$

$$B = \frac{1}{T} \left\{ \frac{y}{3} + \frac{2\gamma}{y} + \frac{t(\delta e^t - 2x^*)}{(e^t-1)^2} + \frac{4x^* t^2 e^t}{(e^t-1)^3} \right\}$$

$$C = 1 + \frac{y}{3} + \frac{2\gamma}{y} + \frac{\delta}{e^t-1} + \frac{2x^* t}{(e^t-1)^2}$$

$$D = \frac{1}{\sigma yT} \ \frac{1+e^{-t}(t-1)}{(1-e^{-t})^2} \quad .$$

Figures B1, B2 and B3 illustrate results obtained for the mole fractions of the major constituents of equilibrium hydrogen for different pressures and temperatures. The constituents H_2^+ and H^- were never significant so results for these species are not shown. It is noted that even for the 10 atmosphere case (Fig. B1) ionization does not begin to become significant until the temperature approaches 12,000 Kelvin. As a test, the calculated values for the thermodynamic properties and the composition were
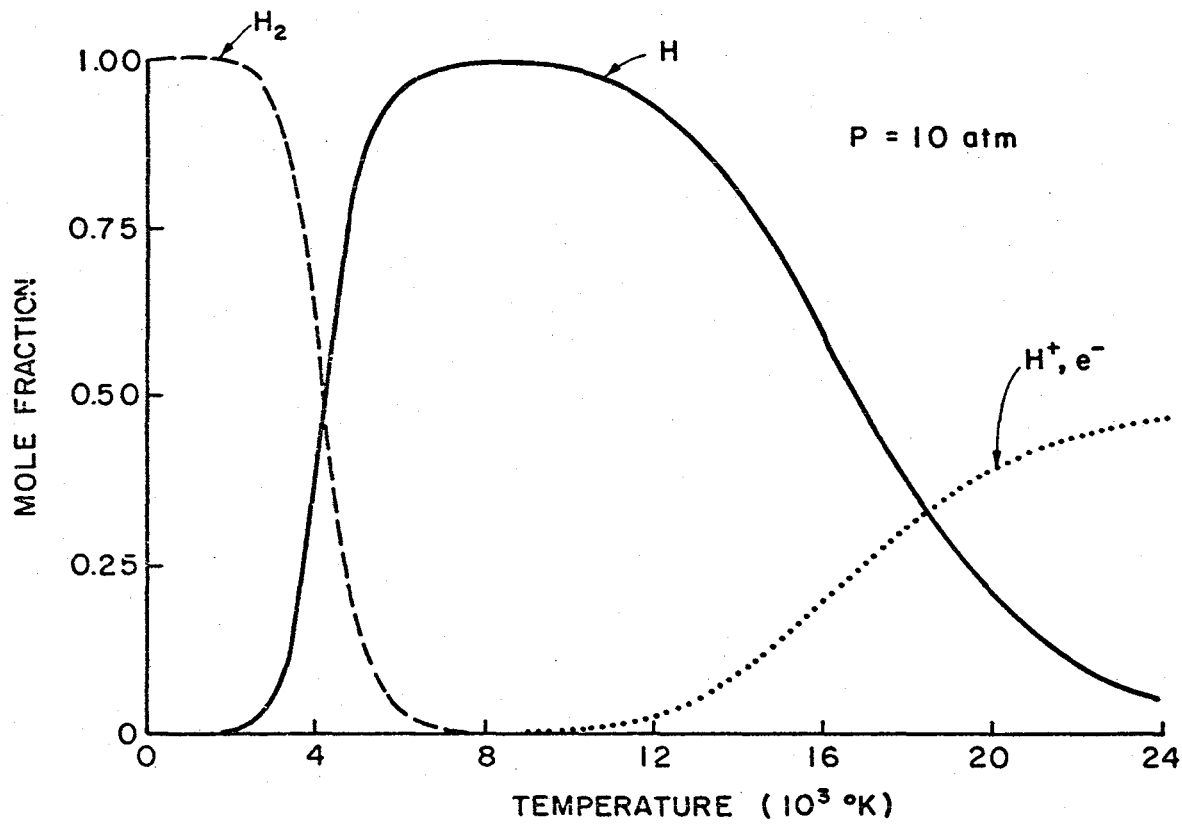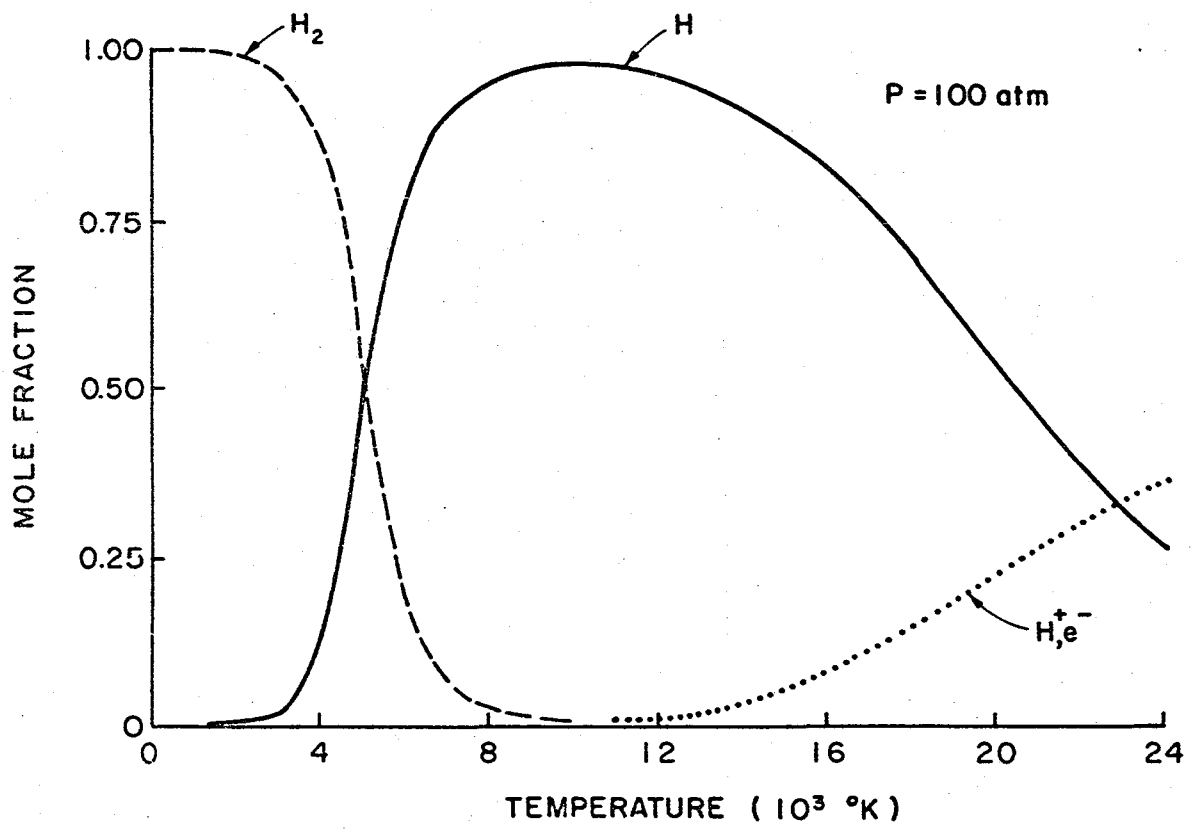
Fig. B1   Equilibrium Hydrogen Composition at 10 Atm

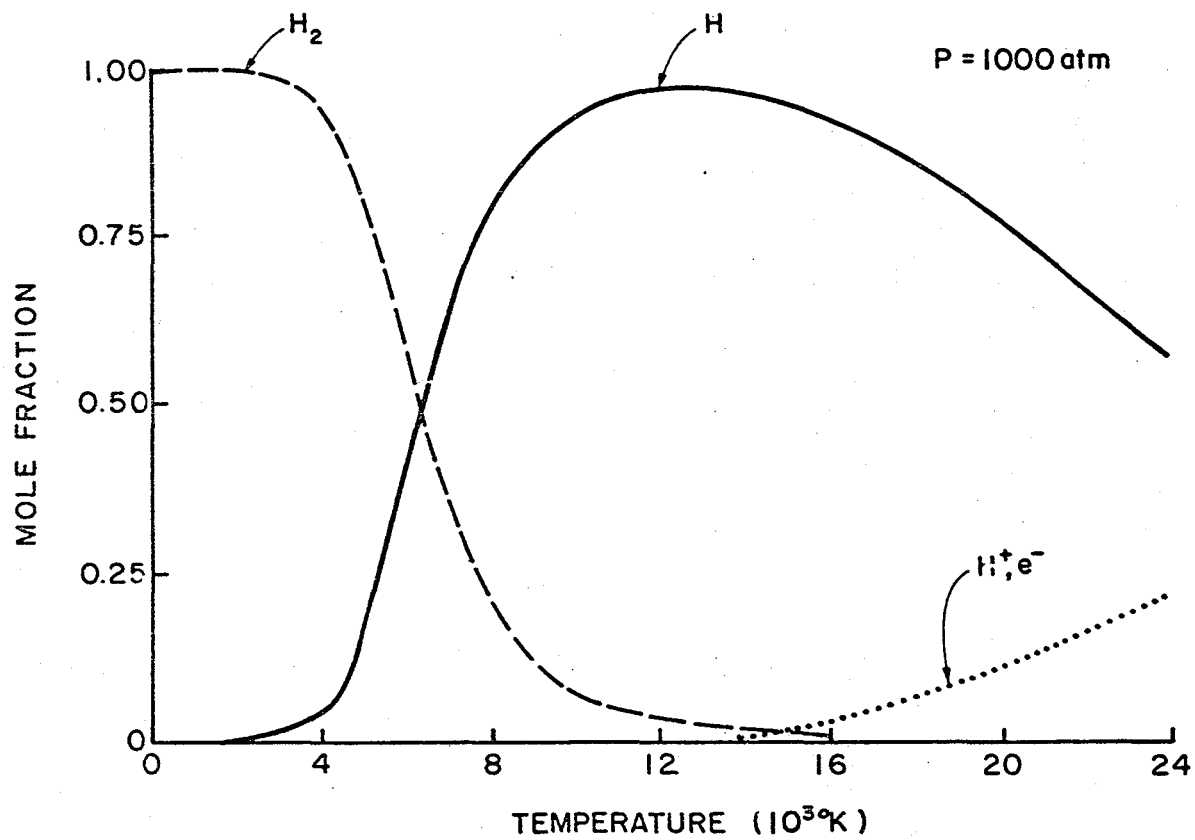Fig. B2   Equilibrium Hydrogen Composition at 100 Atm

Fig. B3 Equilibrium Hydrogen Composition at 1000 Atm

compared to values obtained from Reference B5. In the cases evaluated, the percent differences between the results from Reference B5 and the results calculated were typicall of the order of 1% to 3%. It is recognized that the results of Reference B5 doe not include ionization. However, the excellent agreement between the low-temperature results presented in Reference B5 and those given by the model described here is assumed to indicate high accuracy in the high-temperature regimes as well.

The electrothermal ramjet was typically found to be operating within internal propellant temperature regimes of the order of 10^3 Kelvin and pressure regimes of the order of 10^3 atmospheres and it was found that ionization was typically unimportant for the ramjet operational conditions presented in this thesis.

APPENDIX C

NONEQUILIBRIUM NOZZLE FLOW

APPENDIX C NOMENCLATURE

B = constant used in Eq. 8, 78.01 $\frac{Kmole}{m^3 \, {}^\circ K^{1/2}}$

C_H = mass fraction of H

D_O = H_2 dissociation energy, 7.171×10^{-19} J

H = monatomic hydrogen specie

H_2 = diatomic hydrogen specie

K = Boltzmann's constant, 1.3804×10^{-23} J/${}^\circ K$

K_b = backward rate constant, $\frac{m^6}{Kmole^2 \, sec}$

K_f = forward rate constant, $\frac{m^3}{Kmole \, sec}$

M_H = molecular weight of H, $\frac{Kg}{Kmole}$

N = constant used in Equation 9

R_d = dissociation rate, $\frac{Kmole}{m^3 \, sec}$

R_r = recombination rate, $\frac{Kmole}{m^3 \, sec}$

T = temperature, ${}^\circ K$

t = time, sec

u = velocity, m/s

$\forall$ = volume, m^3

X = distance, m

ρ = density, Kg/m^3

θ_v = harmonic oscillator constant for H_2, $6338.3{}^\circ K$

APPENDIX C

NONEQUILIBRIUM NOZZLE FLOW

In the analysis of supersonic nozzles it is desirable to evaluate the nonequilbrium effects caused by finite rate reactions. This Appendix describes the Bray sudden freezing technique[C1] which was utilized in the analyses presented in this thesis.

The dominant species in this analysis are assumed to be H_2 and H and the following chemical reactions are considered

$$H_2 + H_2 \rightleftharpoons 2H + H_2 \qquad (1)$$

$$H_2 + H \rightleftharpoons 2H + H \quad . \qquad (2)$$

Four body and higher collisions are neglected. The rate equations which are assumed to apply to the above chemical reactions are for Eq. 1

$$\frac{D[H]}{Dt} = 2K_{f_{H_2}} [H_2]^2 - 2K_{b_{H_2}} [H]^2[H_2] \qquad (3)$$

and for Eq. 2

$$\frac{D[H]}{Dt} = 2K_{f_H} [H] [H_2] - 2K_{b_H} [H]^3 \quad . \qquad (4)$$

[H] and [H_2] represent the molar densities of H and H_2 and $K_{f_{H_2}}$ and $K_{b_{H_2}}$ are the corresponding forward and backward rate constants pertaining to Eq. 1. Similarly K_{f_H} and K_{b_H} correspond to Eq. 2. Combining these equations to obtain the net molar production rate for atomic hydrogen yields

$$\frac{D[H]}{Dt} = \left\{ 2K_{f_{H_2}}[H_2]^2 + 2K_{f_H}[H] [H_2] \right\} - \left\{ 2K_{b_{H_2}}[H]^2[H_2] + 2K_{b_H} [H]^3 \right\} \quad . \qquad (5)$$

Defining

$$R_d = 2K_{f_{H_2}} [H_2]^2 + 2K_{f_H} [H] [H_2]$$

$$R_r = 2K_{b_{H_2}} [H]^2[H_2] + 2K_{b_H} [H]^3$$

where R_d represents the rate of dissociation and R_r represents the rate of recombination permits Eq. 5 to be expressed in the form

$$\frac{D[H]}{Dt} = R_d - R_r \ . \tag{6}$$

It should be made clear at this point in the analysis that the previous equation assumes the volume of the hydrogen system does not change with time. The expression for the volumetric substantial derivative is

$$- \frac{[H]}{V} \frac{dV}{dt} \ .$$

The magnitude of this term is assumed to be small compared with R_d and R_r and will therefore be neglected in this analysis.

If the mass fraction of atomic hydrogen (C_H) is defined as the mass of H divided by the total system mass then the time rate of change of C_H for a system can be defined by

$$\frac{DC_H}{Dt} = \frac{D[H]}{Dt} \frac{M_H}{\rho} = (R_d - R_r) \frac{M_H}{\rho} \tag{7}$$

where ρ is the system density (which is assumed to be constant) and M_H is the molecular weight of H.

For a supersonic nozzle operating under quasi-steady conditions the substantial derivative expressing the time rate of change of the mass fraction of H is given by

$$\frac{DC_H}{Dt} = u \frac{\partial C_H}{\partial X}$$

where u is the local velocity and X is the distance downstream from the nozzle entrance.

Consider a supersonic nozzle operating under quasi-steady conditions and assume that equilibrium flow exists up to the nozzle throat. Near the throat the local fluid velocities will be small, the chemical reaction rates will be large, and the characteristic chemical relaxation times will be small compared to the time that it takes a fluid element to move a fractional distance down the nozzle. Consequently the propellant flowfield will be very close to chemical equilibrium, and for this analysis it will be assumed to be in complete equilibrium. As a fluid element accelerates down the nozzle, the molar densities of the species and the local static temperature will drop and these two effects will affect the flowfield significantly. The effect of dropping the molar densities of the reacting species can be seen by examining Eq. 5, which shows that dropping the molar densities decreases the net reaction rate and this in turn increases the characteristic fluid particle chemical relaxation time. The effect of dropping the local static temperature is brought out by considering the forward and backward rate constants used in Eqs. 3 and 4. The backward rate constants used in Eqs. 3 and 4 are respectively

$$K_{b_{H_2}} = \frac{7.5 \times 10^{12}}{T} \quad \frac{m^6}{Kmole^2 \ sec}$$

$$K_{b_H} = \frac{5.9 \times 10^{13}}{T} \quad \frac{m^6}{Kmole^2 \ sec}$$

For either Eq. 3 or Eq. 4 the forward and backward rate constants are related by the following expression

$$\frac{K_f}{K_b} = B \left\{ \exp \left[-\frac{D_0}{KT} \right] \right\} \left\{ \left| 1 - \exp \left[-\frac{\theta_v}{T} \right] \right| \right\} T^{\frac{1}{2}} \qquad (8)$$

where

$$B = 78.01 \frac{Kmole}{m^3 {}^\circ K^{\frac{1}{2}}}$$

$$\frac{D_0}{K} = 51960 \ {}^\circ K$$

$$\theta_v = 6338.3 \ {}^\circ K \ .$$

This equation, which is actually a form of the equilibrium constant for the $H_2 \rightleftharpoons 2H$ reaction, can be derived by using the results of statistical mechanics and by assuming that electronic excitation is not important and that the H_2 molecule behaves as a harmonic oscillator. Examination of Eq. 8 illustrates that as the local static temperature drops, the ratio K_f/K_b becomes small very quickly (this is due to the exponential term involving the chemical energy D_0 which dominates the expression). This effectively causes R_d to become smaller than R_r (hence recombination is favored).

Using these results the Bray sudden freezing criterion can be stated in the following ways

1) Near the throat the flow velocity is not large and the chemical relaxation rates are large because the local temperatures and the reacting specie molar densities are high. In this region the characteristic chemical relaxation times are small compared with the time that it takes a fluid

$\zeta - 2$

element to move a fractional distance down the nozzle and consequently the flow is assumed to be in chemical equilibrium.

2) In the flow downstream of the throat, the molar densities and the temperatures drop while the flow velocity increases. The chemical molar densities lag farther and farther behind the equilibrium values and finite rate reactions begin to become important.

3) The propellant eventually reaches a point where the net rate of chemical reaction is sufficiently small and the local velocity is sufficiently large so that the partial derivative $\partial C_H / \partial X$ becomes small. Downstream of this point in the flowfield the propellant is essentially chemically nonreacting and it is assumed to be fixed in composition (frozen). The characteristic chemical relaxation times are large compared to the time required to tranverse the flowfield.

4) The transition from equilibrium to freezing occurs very quickly within a narrow region, and the location of this region is defined when the following relation is met

$$ u \left| \frac{\partial C_H}{\partial X} \right|_e = \frac{M_H}{\rho} R_d N \qquad (9) $$

where the subscript e denotes equilibrium conditions and N is a constant of the order of unity. This expression states that the narrow freezing region is located at the point where the local substantial derivative of the mass fraction of H is of the same order as the dissociation term appearing in Eq. 6. This implies that R_r is beginning to become larger

than R_d. Consequently, the flow is beginning to depart from chemical equilibrium and the characteristic chemical relaxation times are increasing. A value of unity was used for N in this analysis, which was suggested by Reference C1.

In the analyses conducted it was found that the supersonic nozzle flowfields were typically near chemical equilibrium conditions. This is due to the fact that the propellant is typically operating under high pressure and high temperature conditions and the nozzle expansion ratios are not large. Because vibrational, rotational and translational modes of energy storage equilibrate more readily than chemical phenomena it is argued that these modes will also be near equilibrium conditions. This assumption has been applied throughout this analysis.

APPENDIX D

UNSTEADY GAS DYNAMICS EFFECTS

APPENDIX D NOMENCLATURE

A   =   area, m^2

d   =   diameter, m

F   =   thrust, N

g   =   acceleration due to gravity, 9.8 m/s^2

m   =   ramjet control volume propellant mass, Kg

$\dot{m}$ =   propellant mass flow rate, Kg/s

(mv) = ramjet control volume propellant momentum, Kg m/s

P   =   pressure, Pa

t   =   time, sec

v   =   velocity, m/s

Δ =   denotes change of a variable

δ =   conical diffuser half-angle, degrees

σ =   acceleration, g's

ρ =   propellant density, Kg/m^3

τ =   fluid particle residence time, sec

A subscript on a variable denotes conditions at the corresponding location shown in Fig. D1.

APPENDIX D

UNSTEADY GAS DYNAMICS EFFECTS

The analyses presented thus far in this thesis have assumed that the propellant flow can be considered to be in a quasi-steady state. In reality, however, the flowfield variables will be changing with respect to time as the electrothermal ramjet accelerates down a launch tube, and it is possible that errors will be introduced by assuming quasi-steady flowfields. It is the purpose of this Appendix to present preliminary calculations which address the effects of unsteadiness.

In order to analyze unsteadiness effects it is helpful to consider the residence time (τ) of a typical fluid particle in the ramjet and to estimate the flowfield changes that will occur over this residence time. Values for τ will be calculated from the quasi-steady analyses used to generate the results presented earlier in this thesis. Values for fluid particle residence times are generated by specifying a geometric configuration and calculating the time that it takes a fluid particle to pass through this configuration when the internal propellant velocities relative to the projectile are known. The geometric configuration selected (Figure D1) has a conical half-angle (δ) of 30°, an annular diffuser throat diameter (d_3) of 16 cm, an annular heat addition region diameter (d_4) of 8 cm, a heat addition region length of 1.0 m, and a total projectile length of 1.25 m. Three separate projectile velocity levels of 4000 m/s, 7000 m/s and 15,000 m/s will be examined and one value for the thrust per unit tube area (F/A_1) will be examined for each velocity. For 4000 m/s the thrust per unit tube area is 6.7×10^7 Pa and for 7000 m/s and 15000 m/s the values for the thrust per unit tube area are
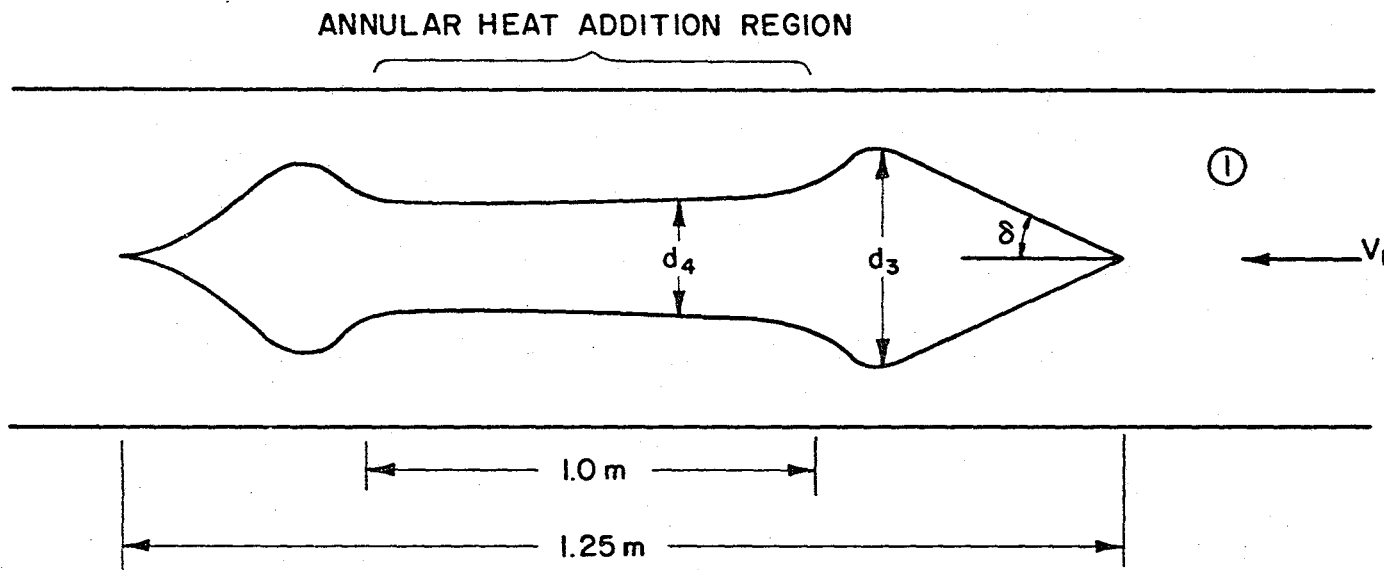
Fig. D1 Electrothermal Ramjet Dimensions

9.5×10^7 Pa and 1.1×10^8 Pa respectively. The calculated fluid particle residence times for 4000 m/s, 7000 m/s and 15000 m/s are respectively

$$\tau_{4000} = 0.769 \times 10^{-3} \text{ sec}$$

$$\tau_{7000} = 1.36 \times 10^{-3} \text{ sec}$$

$$\tau_{15000} = 0.861 \times 10^{-3} \text{ sec.}$$

The values for the non-dimensional thrust that correspond to these three velocities are

$$\left(\frac{F}{P_1 A_1}\right)_{4000} = 6$$

$$\left(\frac{F}{P_1 A_1}\right)_{7000} = 10$$

$$\left(\frac{F}{P_1 A_1}\right)_{15000} = 70.$$

It is noted that the fluid particle residence times are primarily dominated by the length of time that a particle spends in the heat addition region of a ramjet, and in order for the residence times to be calculated with high degrees of accuracy it is necessary that the details of the heat addition be known. Also, increasing the amount of heat added per unit mass of propellant increases the average propellant velocity in the heat addition region. This in turn causes the heat addition region residence time to decrease. This explains why there is no definite trend for the residence times presented earlier. The differences are due primarily to the selection of the heat addition rate per unit mass of propellant, and these residence times were selected as being representative of what could occur in an actual device operating with the geometric configuration specified.

During a residence time (τ) the ramjet velocity (v) will increase by an amount Δv. It is instructive to calculate the ratio $\Delta v/v$, which is the ratio of the change in velocity over the time τ to the velocity of the ramjet at the beginning of the time τ. For constant acceleration this ratio is given by

$$\frac{\Delta v}{v} = \frac{\sigma g \, \tau}{v} \, .$$

Using an acceleration level (σ) of 30,000 g's, which will be used throughout this Appendix, along with the values for the residence times just calculated gives the following normalized changes in projectile velocity

$$\left(\frac{\Delta v}{v}\right)_{4000} = 0.057$$

$$\left(\frac{\Delta v}{v}\right)_{7000} = 0.057$$

$$\left(\frac{\Delta v}{v}\right)_{15000} = 0.017.$$

These values are reasonable and suggest that the projectile velocity will not change significantly during typical fluid particle residence times for an acceleration level of 30,000 g's.

It is also possible that propellant mass and propellant momentum will accumulate within the ramjet control volume, and it is instructive to consider the control volume flowfield changes over the fluid particle residence times. Consider first the possibility of mass accumulation for a projectile undergoing a constant acceleration. At any time t the influx of mass is given by

$$\dot{m}_{in} = A_1 \rho_1 V_1 \quad .$$

The change in the ramjet control volume mass due to the change in the incoming mass flow as the projectile accelerates during the residence time τ can be approximated by

$$\Delta m = (\dot{m}_{t+\tau} - \dot{m}_t) \tau \quad ,$$

and this can be divided by the mass of propellant in the ramjet (m) to determine the ratio $\Delta m/m$ which should be small.

At any time t the momentum flow entering a ramjet control volume is given by

$$\frac{d}{dt} (mv) = \rho_1 A_1 V_1^2 \quad ,$$

where (mv) is the ramjet control volume propellant momentum relative to the ramjet, and the amount of momentum that will enter a ramjet control volume over a residence time τ can be approximated by

$$\Delta(mv) = \left(\frac{d}{dt} (mv)_{t+\tau} - \frac{d}{dt} (mv)_\tau \right) \tau \quad .$$

Again the ratio of this momentum change to the propellant momentum relative to the ramjet (mv) should be small if unsteady effects are to be negligible. Computation of the ratios $\Delta m/m$ and $\Delta(mv)/(mv)$ have been performed and the results are shown below. For each calculation, it has been assumed that the density of the incoming propellant does not change over a residence time (though increases in velocity would ordinarily imply reductions in density).

$$\left(\frac{\Delta m}{m}\right)_{4000} = 3.8 \times 10^{-2}$$

$$\left(\frac{\Delta m}{m}\right)_{7000} = 5.57 \times 10^{-2}$$

$$\left(\frac{\Delta m}{m}\right)_{15000} = 1.32 \times 10^{-2}$$

$$\left(\frac{\Delta(mv)}{(mv)}\right)_{4000} = 0.11$$

$$\left(\frac{\Delta(mv)}{(mv)}\right)_{7000} = 0.45$$

$$\left(\frac{\Delta(mv)}{(mv)}\right)_{15000} = 0.14$$

The above results suggest the errors associated with the changes in mass are not large, while the errors associated with the changes in propellant control volume momentum are more significant. It is noted, however, that proper control of the propellant density immediately upstream of the accelerating ramjet will allow these momentum errors to be reduced. The errors that were estimated are felt to be at the upper limit of what might actually occur and although a complete analysis has not been carried out, intuitively it is felt that the ramjet operational conditions could be controlled in a way that would make these errors insignificant. For example, it is apparent that the propellant density should decrease as ramjet velocity increases so that mass and momentum accumulation will be minimized, and this decrease in density is also required for optimum quasi-steady operation (see Figure 12).

Another area of concern is associated with the fact that the propellant in the heat addition region is being accelerated, and it is possible that a "hydrostatic" pressure gradient could be produced in

the heat addition region. This problem was also analyzed for the cases presented earlier and results for the ratio $\Delta P/P$ were computed. In this ratio ΔP is the "hydrostatic" pressure difference across the heat addition region and P is the average quasi-steady pressure calculated for the heat addition region. Computed values of this ratio are

$$\left(\frac{\Delta P}{P}\right)_{4000} = 0.064$$

$$\left(\frac{\Delta P}{P}\right)_{7000} = 0.028$$

$$\left(\frac{\Delta P}{P}\right)_{15000} = 0.0075 \ .$$

These values are considered not large enough to introduce significant errors into the results presented thus far.

In conclusion, it is felt that the errors incurred by assuming quasi-steady operation, while significant, are not sufficiently large to suggest the results presented are grossly in error. Further it is suggested that these errors can be reduced significantly by proper launch trajectory design. It is also noted that these results were obtained for a specific geometric configuration and acceleration level. Decreasing the various dimensions presented earlier and decreasing the acceleration level will decrease the errors associated with unsteady gas dynamics effects.

End of Document